# Liver acid sphingomyelinase inhibits growth of metastatic colon cancer

Yosuke Osawa,[1,2,3] Atsushi Suetsugu,[2] Rie Matsushima-Nishiwaki,[1] Ichiro Yasuda,[2] Toshiji Saibara,[4] Hisataka Moriwaki,[2] Mitsuru Seishima,[3] and Osamu Kozawa[1]

[1]Department of Pharmacology, [2]Department of Gastroenterology, and [3]Department of Informative Clinical Medicine, Gifu University Graduate School of Medicine, Gifu, Japan. [4]Department of Gastroenterology and Hepatology, Kochi University School of Medicine, Kochi, Japan.

**Acid sphingomyelinase (ASM) regulates the homeostasis of sphingolipids, including ceramides and sphingosine-1-phosphate (S1P). These sphingolipids regulate carcinogenesis and proliferation, survival, and apoptosis of cancer cells. However, the role of ASM in host defense against liver metastasis remains unclear. In this study, the involvement of ASM in liver metastasis of colon cancer was examined using *Asm*$^{-/-}$ and *Asm*$^{+/+}$ mice that were inoculated with SL4 colon cancer cells to produce metastatic liver tumors. *Asm*$^{-/-}$ mice demonstrated enhanced tumor growth and reduced macrophage accumulation in the tumor, accompanied by decreased numbers of hepatic myofibroblasts (hMFs), which express tissue inhibitor of metalloproteinase 1 (TIMP1), around the tumor margin. Tumor growth was increased by macrophage depletion or by *Timp1* deficiency, but was decreased by hepatocyte-specific ASM overexpression, which was associated with increased S1P production. S1P stimulated macrophage migration and TIMP1 expression in hMFs in vitro. These findings indicate that ASM in the liver inhibits tumor growth through cytotoxic macrophage accumulation and TIMP1 production by hMFs in response to S1P. Targeting ASM may represent a new therapeutic strategy for treating liver metastasis of colon cancer.**

## Introduction

Colon cancer, one of the most common malignancies, frequently metastasizes to the liver. Acid sphingomyelinase (ASM) is involved in various physiological cellular functions and diseases, including cancer (1), and hydrolyzes sphingomyelin into ceramide and phosphorylcholine. Ceramide, a bioactive mediator of numerous cellular functions, such as apoptosis and cell cycle regulation (2, 3), is in turn hydrolyzed by ceramidase into sphingosine, which is subsequently phosphorylated into sphingosine-1-phosphate (S1P) by sphingosine kinase (SphK). Although these sphingolipids are involved in colon carcinogenesis and colon cancer cell survival (4, 5), the roles of ASM and S1P in host antitumor defenses (i.e., inhibiting the progression of colon cancer metastasis to the liver) remain unclear.

Tumors contain stromal cells, such as immune cells and fibroblasts (6). Infiltrated tumor-associated macrophages (TAMs) have recently been reported to function as promoters of tumor progression (7–9), with several clinical studies demonstrating an association between the presence of TAMs and poor prognosis in various cancers (10). In contrast, opposing data have shown that the presence of TAMs is correlated with improved survival and that these cells have protective potential in colon cancer (11, 12). Although tumor growth–promoting TAMs have been observed to resemble regulatory M2 macrophages (13, 14), the density of classically activated M1 macrophages is positively correlated with the survival time of patients with non–small-cell lung cancer (15). These findings indicate that macrophages have contrasting roles in cancer, depending on their phenotype (13).

S1P is a ceramide-derived metabolite that is involved in various cellular functions and increases migration of macrophages (16, 17), resulting in macrophage recruitment. S1P released from apoptotic tumor cells induces a switch from the M1 to the M2 macrophage subtype (18). In contrast, the S1P analog FTY720 does not alter the ratio of M1 and M2 subtypes in mouse peritoneal macrophages (19). Because of these contrasting findings, the effect of S1P on macrophages remains controversial and poorly understood. Whereas MMP cleavage of the ECM, a primary barrier against tumor invasion produced by hepatic myofibroblasts (hMFs) in the liver, promotes cancer cell migration, invasion, and metastasis, MMP inhibitors reduce colon cancer metastasis to the liver (20). Specifically, overexpression of tissue inhibitors of metalloproteinases (TIMPs), endogenous inhibitors of MMPs, inhibits liver metastasis of colon cancer in animal models (21), whereas decreased TIMP1 expression in the liver results in progression of SV40T antigen–induced hepatocellular carcinoma (22) and increased metastatic colonization of T cell lymphoma (23). However, it has been reported that elevated TIMP levels are associated with cancer progression (24). Thus, although S1P stimulates hMF accumulation and TIMP1 induction in the liver (25, 26), the precise roles of S1P in tumor growth remain unclear. To attempt to clarify these precise roles, we here investigated the involvement of ASM in the progression of liver metastasis of colon cancer.

## Results

*Role of ASM deficiency and overexpression in the progression of metastatic liver tumors of colon cancer.* To determine the role of host ASM on metastatic liver tumor growth caused by colon cancer, we created metastatic liver tumors by intrasplenic injection with SL4 cells, a mouse colon cancer cell line, and examined expression of ASM and ceramide by immunostaining. ASM and ceramide expression increased in the liver cells around the tumors (Supplemental Figure 1A; supplemental material available online with this article; doi:10.1172/JCI65188DS1), which suggests that tumor cells stimulate ASM expression and promote its activity in liver cells. To examine the effect of ASM deficiency on metastatic liver tumors, the extent of tumor growth in *Asm*$^{+/+}$ and *Asm*$^{-/-}$ mice

**Conflict of interest:** The authors have declared that no conflict of interest exists.

**Citation for this article:** *J Clin Invest.* doi:10.1172/JCI65188.

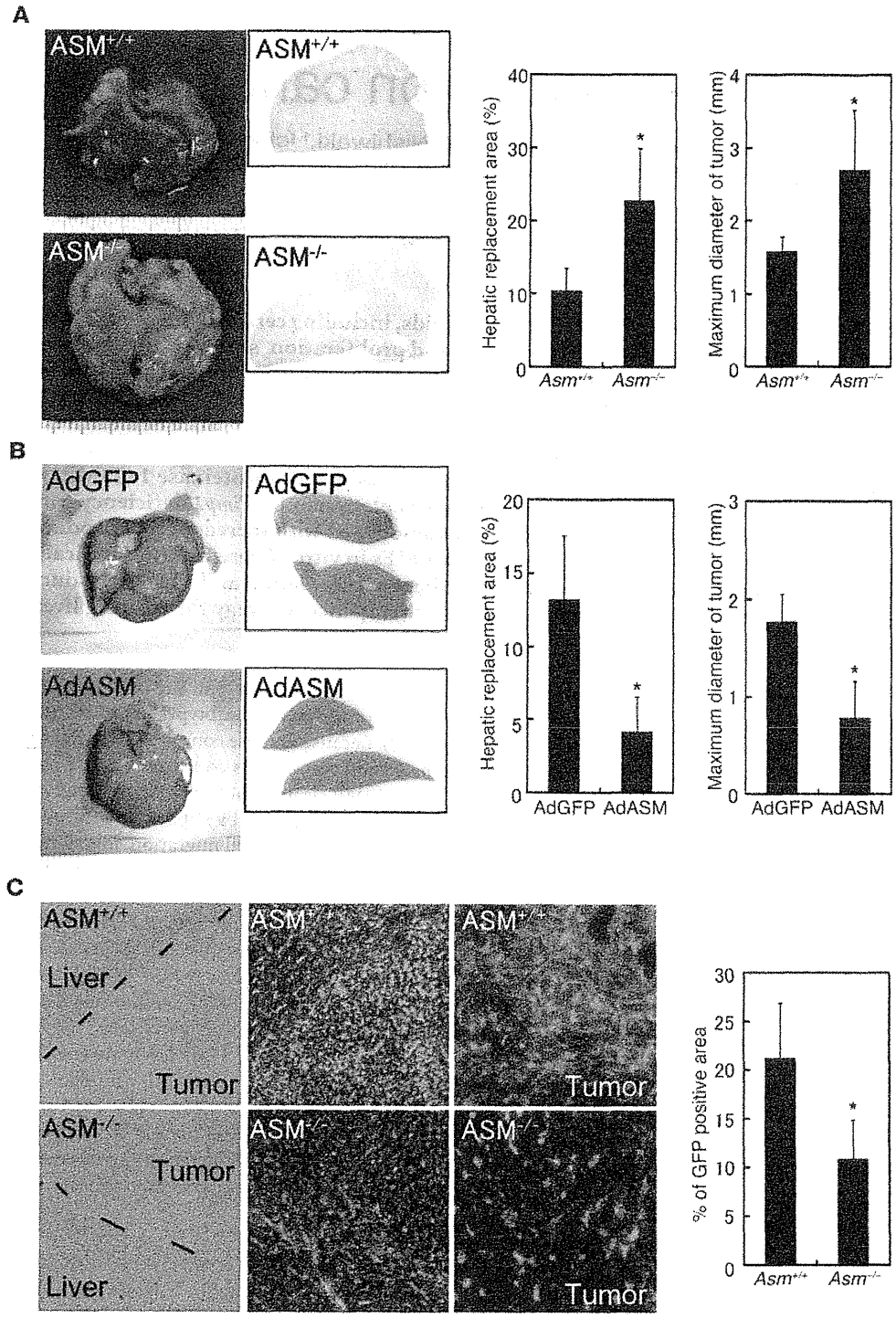


**Figure 1**
ASM deficiency increased, and ASM overexpression decreased, metastatic tumor growth in the liver. (**A** and **B**) $Asm^{+/+}$ and $Asm^{-/-}$ mice were intrasplenically injected with $2 \times 10^4$ SL4 cells (**A**). Wild-type mice were infected with AdGFP or AdASM 24 hours before inoculation (**B**). Mice were sacrificed 14 days after inoculation, and livers were excised and photographed. Liver sections were stained with H&E (loupe magnification), and intrahepatic tumor load was presented as hepatic replacement area and maximum diameter, based on measurement of 3 nonsequential sections. (**C**) $GFP^+Asm^{+/+}$ and $GFP^+Asm^{-/-}$ mice were intrasplenically injected with SL4 cells. At 14 days after inoculation, GFP expression in the liver was assessed by fluorescent microscopy, measurement of the $GFP^+$ area was performed, and nuclei were stained with DAPI. Shown are bright field images at the border of the metastatic tumor and liver (left), GFP/DAPI merge in the same bright field images (middle), and higher-magnification views of GFP/DAPI merge in the tumor area (right). Original magnification, ×200 (left and middle); ×400 (right). Results are mean ± SD of data obtained from at least 5 independent experiments. $^*P < 0.05$, 2-tailed Student's *t* test.

was compared. No tumors were evident in livers without SL4 cell inoculation (Supplemental Figure 1B). After inoculation with SL4 cells, the hepatic replacement area, maximum tumor diameter, and liver weight were increased in $Asm^{-/-}$ compared with $Asm^{+/+}$ mice (Figure 1A and Supplemental Figure 1C). In contrast, a similar number of the initially transplanted cells was observed in the livers of $Asm^{+/+}$ and $Asm^{-/-}$ mice 6 hours after inoculation (Supplemental Figure 2A). These results indicate that colon cancer cells grow more rapidly in the $Asm^{-/-}$ liver. Conversely, administration of adenovirus-expressing ASM (AdASM) to the mice prior to cancer cell inoculation inhibited tumor growth compared with adenovirus-expressing GFP (AdGFP) administration (Figure 1B). AdASM-derived GFP was expressed in the hepatocytes, but not in the tumor cells (Supplemental Figure 2B). In support of the results of our previous study (27), AdASM increased ASM activity in the liver (Supplemental Figure 2C). In addition, ASM-chimeric mice,

in which ASM was deficient only in bone marrow–derived cells, demonstrated tumor growth that was comparable to mice containing *Asm*$^{+/+}$ bone marrow cells (Supplemental Figure 3A). These results indicate that ASM in hepatocytes, but not in bone marrow–derived cells, is involved in the inhibition of tumor growth.

To explore the mechanisms of enhanced tumor growth in *Asm*$^{-/-}$ mice, we generated *GFP*$^{+}$*Asm*$^{-/-}$ mice and examined the host-tumor interaction by inoculating *GFP*$^{+}$*Asm*$^{+/+}$ and *GFP*$^{+}$*Asm*$^{-/-}$ mice with SL4 cells. After inoculation, spindle-shaped host-derived *GFP*$^{+}$ cells, most of which expressed F4/80 (Figure 2A), were observed in the metastatic liver tumors, while fewer host-derived cell infiltrates were observed in the *Asm*$^{-/-}$ livers (Figure 1C). Spindle-shaped bone marrow–derived cells were also observed in the tumors of GFP-chimeric mice (expressing GFP only in bone marrow–derived cells; Supplemental Figure 3B), which suggests that these cells were F4/80$^{+}$ macrophages originating from the bone marrow. F4/80$^{+}$ cells were observed in the tumors; compared with the control livers, a smaller number of F4/80$^{+}$ cells was observed in the *Asm*$^{-/-}$ livers, while a greater number of these cells was present in AdASM-infected livers (Figure 2, B and C). The induction of classically activated M1 macrophage markers (*Cd11c*, *Il12p40*, and *Ifng*) by SL4 cell inoculation was more remarkable than that of *Cd163*, mannose receptor, and *Il10*, markers for regulatory M2 macrophages (Supplemental Table 1). Thus, these findings suggested that the accumulated macrophages were M1 dominant. In *Asm*$^{+/+}$ mice transplanted with *GFP*$^{+}$*Asm*$^{-/-}$ bone marrow, the number of bone marrow–derived *GFP*$^{+}$*Asm*$^{-/-}$ cells in the tumor was comparable to that of *GFP*$^{+}$*Asm*$^{+/+}$ cells in the control *Asm*$^{+/+}$ mice transplanted with *GFP*$^{+}$*Asm*$^{+/+}$ bone marrow (Supplemental Figure 3C). Therefore, it is likely that ASM in hepatocytes, but not in bone marrow–derived cells, contributes to the accumulation of macrophages in tumors.

To examine whether macrophage accumulation in tumors is involved in the inhibition of tumor growth, liposome-encapsulated alendronate was administered to the SL4 cell–inoculated mice to decrease the number of F4/80$^{+}$ cells in the tumors (Supplemental Figure 3D). Alendronate administration increased the severity of tumor growth by inducing macrophage depletion (Figure 2D), which is suggestive of macrophage involvement in tumor growth suppression. These data indicate that hepatocytic ASM leads to accumulation of antitumor macrophages in the metastatic liver tumors of colon cancer, thereby suppressing tumor growth.

*Macrophage-induced hMFs accumulate around invasive margins of metastatic liver tumors.* Macrophages have been shown to exhibit antitumor potential as tumoricidal cells and major antigen-presenting cells (28–31). Liver macrophages also modulate the host immune response to cancer cells by releasing cytotoxic products and immune-stimulating factors, including IFN-γ. In accordance with these findings, CD3$^{+}$ lymphocytes infiltrated into the tumors, and fewer CD3$^{+}$ cells were observed in *Asm*$^{-/-}$ and alendronate-treated mice (Supplemental Figure 4, A and B). Moreover, a NKT cell activator, α-galactosylceramide, suppressed tumor growth, even in *Asm*$^{-/-}$ mice (Supplemental Figure 4C), which suggests that the antitumor immunity of NKT cells was not impaired in *Asm*$^{-/-}$ mice. Thus, NKT cells contributed to the antitumor defense mechanism.

Activated macrophages release various types of inflammatory cytokines and growth factors. Among these, TNF-α is thought to induce tumor necrosis. However, in the model used in this study, mRNA expression of *Tnfa* was comparable in SL4 cell–inoculated *Asm*$^{-/-}$ and *Asm*$^{+/+}$ livers (Supplemental Table 2), and tumor growth was not increased in *Tnfa*$^{-/-}$ mice (Supplemental Figure 4D), which suggests that TNF-α is not involved in tumor development in *Asm*$^{-/-}$ mice. The reduced induction of *Il1b*, *Cxcl1*, and *Tgfb* mRNA expression by SL4 cell inoculation in *Asm*$^{-/-}$ compared with *Asm*$^{+/+}$ livers (Supplemental Table 2) can be explained by the reduction in the number of macrophages in the *Asm*$^{-/-}$ liver, as these factors are released from liver macrophages. The mRNA expression levels of *Des* (encoding desmin, a marker of hMFs), *Acta2* (encoding α-SMA, a marker of activated hMFs), and *Col1a1* (encoding collagen α1[I], a product of activated hMFs) were also increased after SL4 cell inoculation in *Asm*$^{+/+}$ livers (Supplemental Table 2), which suggests that the metastatic tumors stimulated hMF proliferation and activation. In the SL4 cell–inoculated mice, the number of desmin$^{+}$ and α-SMA$^{+}$ cells were increased around the invasive margins of the tumors in the liver (Figure 3). Desmin$^{+}$ cells were observed to express GFP in the *GFP*$^{+}$ mice, but not in the GFP-chimeric mice (data not shown), which suggests that the hMFs were derived from host, not from bone marrow. The increase of *Des*, *Acta2*, and *Col1a1* mRNA after SL4 cell inoculation was lower in *Asm*$^{-/-}$ than in *Asm*$^{+/+}$ livers (Supplemental Table 2). Moreover, whereas the number of desmin$^{+}$ and α-SMA$^{+}$ cells was decreased by *Asm* deficiency (Figure 3A) and by macrophage depletion (Figure 3C), it was increased by ASM overexpression (Figure 3B). These findings suggest that increased macrophage accumulation in the metastatic liver tumor by ASM stimulates hMF accumulation and activation. Because the number of desmin$^{+}$ and α-SMA$^{+}$ cells was inversely correlated with tumor growth, we concluded that hMFs may contribute to tumor suppression.

*Role of TIMP1 produced by hMFs in growth suppression of metastatic liver tumors.* Although it has been reported that hMFs contribute to cancer progression, the model used in this study indicated that increased hMF accumulation is negatively correlated with tumor growth. This finding led us to hypothesize that hMFs contain antitumor factors that are increased in number and magnitude by ASM overexpression and decreased by ASM deficiency. To test this hypothesis, we focused on examining TIMP1, which exhibits antitumor potential (21) and is expressed by hMFs (32). In the metastatic tumors, most of the desmin$^{+}$ cells showed double staining for TIMP1 (Figure 4A), which suggests that hMFs are TIMP1$^{+}$. *Timp1* mRNA expression increased in *Asm*$^{+/+}$ livers by SL4 cell inoculation, an increase that was attenuated in *Asm*$^{-/-}$ livers (Figure 4B). Nevertheless, the expression levels of *Mmp2*, *Mmp9*, and *Mmp13* were comparable in *Asm*$^{+/+}$ and *Asm*$^{-/-}$ livers (Supplemental Table 2). The increased number of TIMP1$^{+}$ cells observed around the invasive margin of the tumors was attenuated by *Asm* deficiency as well as by macrophage depletion (Figure 4, C and E), whereas ASM overexpression further increased TIMP1$^{+}$ cell number (Figure 4D), similar to our findings with respect to hMF induction. These results, in addition to the increased tumor growth observed in *Timp1*$^{-/-}$ mice (Figure 4F), suggest that the increased expression of TIMP1 in hMFs by metastatic tumors is involved in the suppression of tumor growth.

*ASM suppression of tumor growth via S1P production.* In accordance with previous reports that ASM hydrolyzes sphingomyelin into ceramide, which is then hydrolyzed by ceramidase and phosphorylated by SphK to form S1P, we observed the level of S1P to increase in AdASM-infected livers (Figure 5A). Although exogenous administration of S1P did not affect *Tnfa*, *Il1b*, *Cxcl1*, *Tgfb*, *Il12p40*, or *Il10* mRNA expression in isolated peritoneal CD11b$^{+}$ macrophages (Supplemental Table 3), these cells showed increased migration toward S1P (Figure 5B), as previously reported regarding RAW 264.7 macrophages (33). These findings suggest that macrophage accumulation in tumors might be caused by S1P-induced macrophage recruitment. Although it

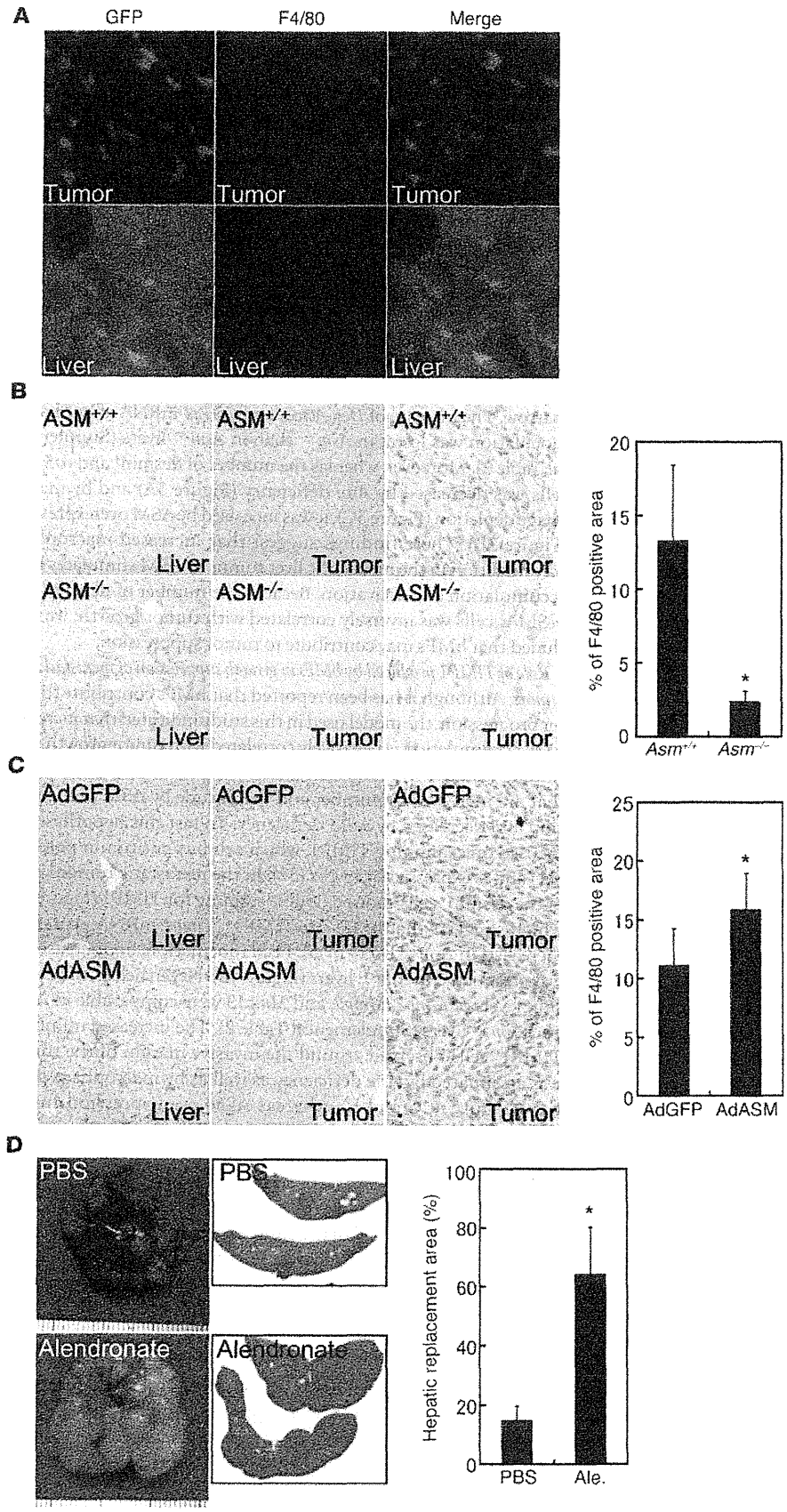


**Figure 2**
Macrophage depletion increased metastatic tumor growth in the liver. (**A**) *GFP*+ mice were intrasplenically injected with 2 × $10^4$ SL4 cells. GFP fluorescence was visualized with fluorescent microscopy, and macrophages were detected in metastatic tumor and liver by immunofluorescent staining for F4/80 (blue). Original magnification, ×400. (**B** and **C**) $Asm^{+/+}$ and $Asm^{-/-}$ mice (**B**) and AdGFP- and AdASM-infected wild-type mice (**C**) were intrasplenically injected with 2 × $10^4$ SL4 cells. Expression of F4/80 in the liver and metastatic tumor was examined by immunohistochemistry with an anti-F4/80 antibody to assess the number of macrophages. Original magnification, ×100 (left and middle); ×400 (right). (**D**) Wild-type mice were injected with SL4 cells and treated with PBS or alendronate before sacrifice 14 days after inoculation. Images of livers after excision and liver sections stained with H&E (loupe magnification) are shown. Intrahepatic tumor load is presented as hepatic replacement area, based on measurement of 3 nonsequential sections. Results are mean ± SD of data collected from at least 5 independent experiments. *$P < 0.05$, 2-tailed Student's *t* test.

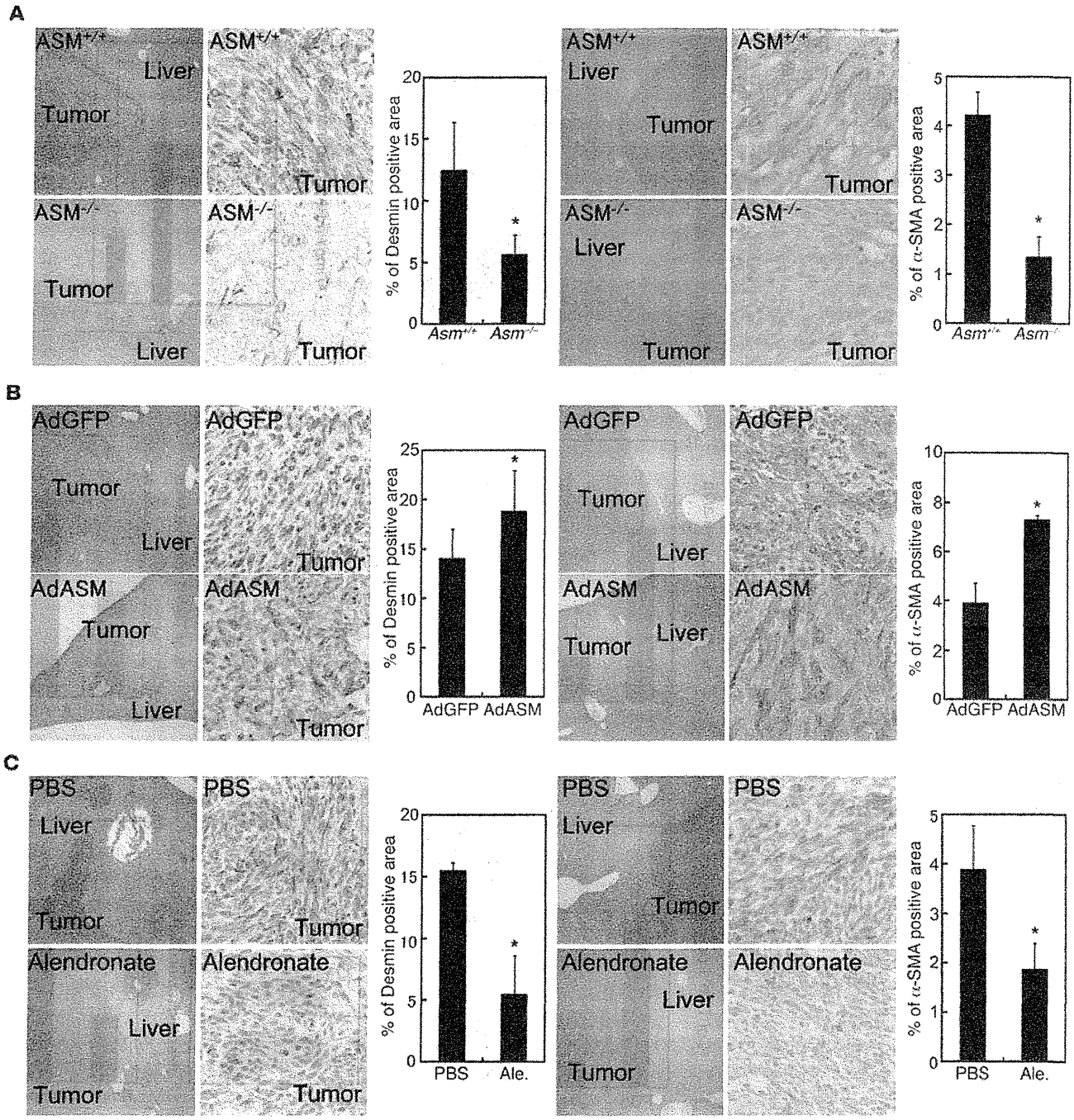


**Figure 3**

ASM deficiency or macrophage depletion decreased hMFs, and ASM overexpression increased hMFs, around the tumor invasive margin. *Asm*$^{+/+}$ and *Asm*$^{-/-}$ mice (**A**), AdGFP- or AdASM-infected wild-type mice (**B**), and wild-type mice treated with PBS or alendronate (**C**) were intrasplenically injected with $2 \times 10^4$ SL4 cells and sacrificed 14 days after inoculation. Expression of desmin (left) and α-SMA (right) around the tumor invasive margin was examined by immunohistochemistry, and measurement of immunostain-positive area was performed. Original magnification, ×40 (left); ×400 (right). Results are mean ± SD of data collected from at least 5 independent experiments. *$P < 0.05$, 2-tailed Student's *t* test.

has been reported that S1P induces a switch from the M1 to the M2 macrophage subtype (18), in the present study, S1P did not alter the mRNA expression levels of M1 and M2 markers, which suggests that S1P does not affect the macrophage phenotype. Instead, our observations that 1 μM S1P treatment for 72 hours increased *Timp1* mRNA expression in isolated hMFs (Figure 5C) and that adenoviral overexpression of SphK1 (AdSphK) in hepatocytes prior to cancer cell inoculation inhibited tumor growth (Supplemental Figure 5A) suggest that ASM suppresses tumor growth via S1P production. The fold increase of *Timp1* mRNA induced by S1P did not seem to

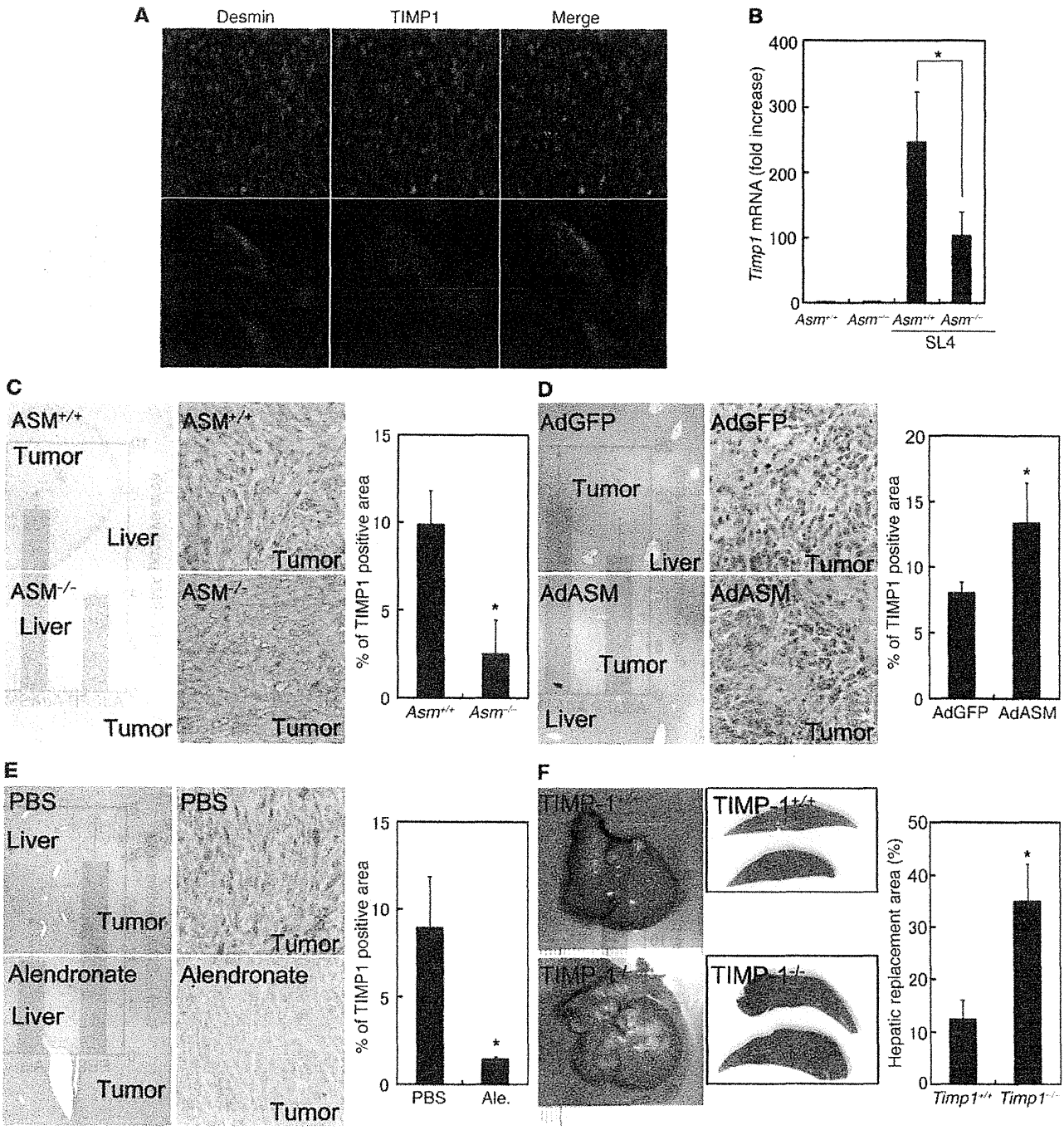


**Figure 4**

TIMP1 deficiency increased metastatic tumor growth in the liver. (**A**) Wild-type mice were intrasplenically injected with $2 \times 10^4$ SL4 cells and sacrificed 14 days after inoculation. Expression of desmin (green) and TIMP1 (red) around the invasive margin of the tumors was examined by immunofluorescent staining. Nuclei were stained with DAPI (blue, top). Original magnification, ×400 (top); ×1,600 (bottom). (**B**) *Asm*$^{+/+}$ and *Asm*$^{-/-}$ mice were intrasplenically injected with $5 \times 10^5$ SL4 cells and sacrificed 7 days after inoculation. *Timp1* mRNA expression in the liver was determined by quantitative real-time RT-PCR. (**C**–**E**) *Asm*$^{+/+}$ and *Asm*$^{-/-}$ mice (**C**), AdGFP- or AdASM-infected wild-type mice (**D**), and wild-type mice treated with PBS or alendronate (**E**) were intrasplenically injected with $2 \times 10^4$ SL4 cells and sacrificed 14 days after inoculation. TIMP1 expression around the tumor invasive margin was examined by immunohistochemistry, and measurement of TIMP1$^+$ area was performed. Original magnification, ×40 (left); ×400 (right). (**F**) *Timp1*$^{+/+}$ and *Timp1*$^{-/-}$ mice were intrasplenically injected with $2 \times 10^4$ SL4 cells and sacrificed 14 days after inoculation. Images of livers after excision and liver sections stained with H&E (loupe magnification) are shown. Intrahepatic tumor load is presented as hepatic replacement area, based on measurement of 3 nonsequential sections. Results are mean ± SD of data collected from at least 5 independent experiments. *$P < 0.05$, 2-tailed Student's *t* test.

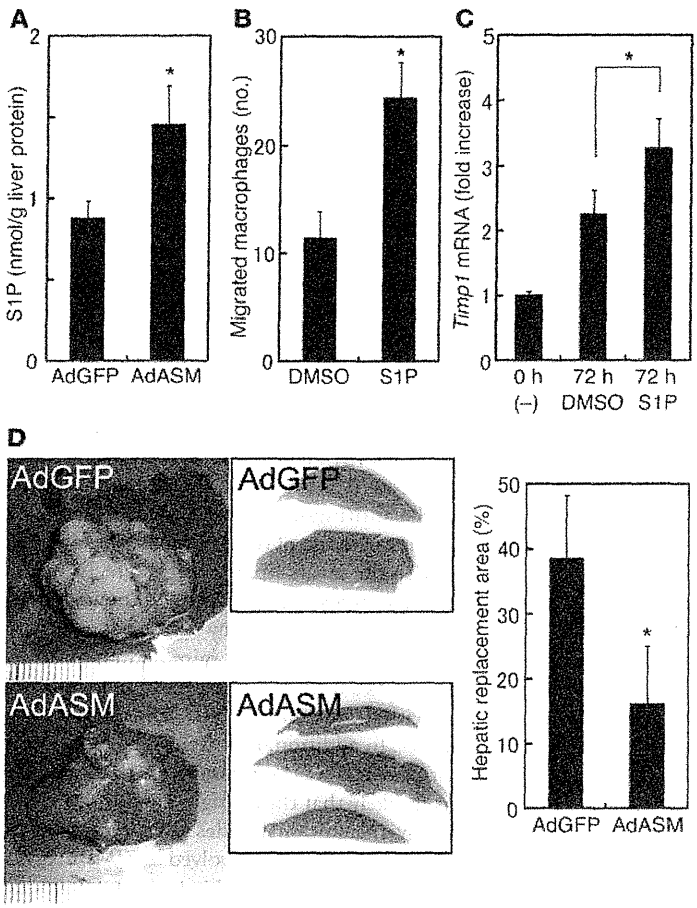


**Figure 5**

S1P promoted macrophage migration and *Timp1* mRNA expression in hMFs. (**A**) Wild-type mice were infected with AdGFP or AdASM, and S1P was examined by MS analysis 3 days after infection. (**B**) After addition of CD11b$^+$ peritoneal macrophages and 1 μM S1P to the upper and lower chambers, respectively, of transwell plates, cells were incubated for 4 hours. The number of macrophages that migrated to the underside of the chamber was determined. (**C**) Primary rat hMFs were incubated with or without 1 μM S1P on plastic dishes for 72 hours before determination of *Timp1* mRNA levels by quantitative real-time RT-PCR. (**D**) Wild-type mice were intrasplenically injected with $2 \times 10^4$ SL4 cells, infected with AdGFP or AdASM 5 days after inoculation, and sacrificed 14 days after infection (i.e., 19 days after inoculation). Images of livers after excision and liver sections stained with H&E (loupe magnification) are shown. Intrahepatic tumor load is presented as hepatic replacement area, based on measurement of 3 nonsequential sections. Results are mean ± SD of data collected from 4 (**A**) or at least 5 (**B–D**) independent experiments. $^*P < 0.05$, 2-tailed Student's *t* test.

be large (Figure 5C). However, a 48-hour treatment with TGF-β has previously been reported to induce an approximately 2-fold increase of *TIMP1* mRNA in cultured human hMFs (34). This suggests that the induction of *Timp1* mRNA by S1P was not a small change, and it is possible that the induction might be sufficient. 5 μM S1P induced TIMP1 expression to a similar degree as that observed using 1 μM S1P (data not shown), which suggests that 1 μM S1P fully induces activation of S1P receptors.

As described above, ASM exerted an antitumor effect through macrophage accumulation and TIMP1 production from hMFs via S1P. To evaluate AdASM administration as a form of treatment against metastatic liver tumors of colon cancer, AdASM was administered to mice 5 days after SL4 cell inoculation. AdASM suppressed tumor growth, even when it was administered after cell inoculation (Figure 5D). However, AdSphK administration did not suppress tumor growth (Supplemental Figure 5B), although the accumulation of F4/80$^+$ and desmin$^+$ cells was similar to that in AdASM-treated mice (Supplemental Figure 6A). In addition, accumulation of F4/80$^+$ and desmin$^+$ cells was observed to be equal, regardless of whether mice were infected with AdSphK before or after SL4 cell inoculation (data not shown). Adenovirus-mediated GFP expression was observed in the tumors when the virus was administered after cell inoculation (Supplemental Figure 6B), which suggests that the adenovirus infects not only hepatocytes, but also inoculated SL4 cells. The observation that AdSphK increased proliferation of cultured SL4 cells (Supplemental Figure 6C) indicated that the antitumor effects of overexpressed SphK1 in the liver may be counteracted by the tumor-promoting effects of SphK1 on SL4 cell proliferation.

## Discussion

In the present study, we investigated the contribution of ASM to the suppression of tumor growth in liver metastasis of colon cancer cells. Our results indicated that liver ASM inhibits tumor growth through S1P formation and subsequent macrophage accumulation and TIMP1 production from hMFs. These results suggest novel therapeutic possibilities for treating metastatic liver tumors of colon cancer.

ASM in cancer cells is involved in cell death and plays an important role in the host response to a variety of anticancer treatments, including those for colon cancer (1). In the present study, metastatic tumors of colon cancer cells stimulated ASM expression and ceramide in liver cells. Moreover, host ASM deficiency increased, while overexpression of ASM in the liver decreased, the growth of liver tumors after inoculation with colon cancer cells, which suggests that ASM in host cells contributes to antitumor defense. Among the roles that ASM plays in liver cells, ASM in hepatocytes stimulates glucose uptake, resulting in improvement of glucose tolerance in mice through S1P production (27). ASM has pleiotropic signaling functions related to posttranslational processing of ASM, and secretory and lysosomal ASM (35) may have distinct functions. Although it is unclear which type of ASM was

involved in S1P production in our study, hepatocytes represented one source of S1P, as the S1P elevation by AdASM was inhibited in both SphK1-deficient livers and SphK1-deficient primary cultured rat hepatocytes (data not shown). Previous studies have shown that the generated S1P can be secreted and act as a ligand for S1P receptors (S1PRs; refs. 27, 36, 37), while the S1P/S1PR1 axis controls the trafficking and migration of immune cells, including macrophages (16, 17, 36). In accordance with these prior reports, S1P increased the migration of peritoneal macrophages in vitro, with less and more macrophage accumulation, respectively, in the tumors of *Asm*$^{-/-}$ and AdASM-infected mice compared with controls. These findings indicate that ASM in hepatocytes leads to macrophage accumulation in tumors via S1P production and that this process exerts an antitumor effect, in contrast to macrophage depletion. Although it has been reported that TAMs, which resemble regulatory M2 macrophages (13, 14), function as promoters of tumor progression (7–9), the macrophages in the tumors inoculated with SL4 colon cancer cells in this study were M1 dominant. It has been proposed that a gradual shift of TAM polarization from the M1 to the M2 subtype occurs during different stages of tumor progression, due to dynamic changes in the tumor microenvironment (38), and is paralleled by the gradual inhibition of NF-κB (39). In this study, we observed immunofluorescent staining of NF-κB p65 in the nuclei of F4/80$^+$ cells in the tumors (data not shown), which suggests that NF-κB is activated in these macrophages. This finding may indicate that in metastatic liver tumors characterized by rapid growth, such as by increased numbers of SL4 cells (40), the accumulated TAMs may retain an M1 phenotype that displays a cytotoxic proinflammatory phenotype. Thus, the number of macrophages present in the tumor is inversely correlated with tumor growth.

Myofibroblasts represent another important component of the tumor stroma; these cells are driven by migration and proliferation-stimulating factors released from cancer cells. Whereas some studies have reported a supportive role for myofibroblasts in cancer cell development (41) and a direct correlation between their presence and poor prognosis (42), others have reported a protective role of myofibroblasts against cancer cells (43, 44), with p53 in stromal fibroblasts demonstrated to inhibit tumor growth and malignant progression (45). In the current study using SL4 cell inoculation, hMF accumulation was found to be dependent on macrophage accumulation and inversely correlated with tumor growth. Specifically, hMF accumulation was increased only around the invasive margins of the tumors, and no hMF infiltration or collagen deposition was observed in the central part of tumors (data not shown). These findings indicate that the supportive effects of hMFs in tumor growth may be limited. However, the observation of enhanced tumor growth in *Timp1*$^{-/-}$ mice indicates that TIMP1 produced from hMFs, stimulated by S1P, might inhibit tumor growth through inhibition of ECM degradation. Although previous studies reported a protumor role for TIMP1, TIMP1 staining was observed only around the tumor invasive margin in the current study, which indicates that the supportive effects of TIMP1 in tumor growth may also be limited.

Whereas ceramide acts as a signaling molecule in the induction of cell responses, such as apoptosis and growth arrest (3, 46, 47), S1P acts as a potent mitogen for a variety of cell types (48), with SphK1/S1P contributing to colon carcinogenesis (49). Ceramide levels in colon carcinoma tissue are significantly lower than those in normal tissue (50), reflecting the fact that the dynamic balance between intracellular levels of ceramide and S1P (the "ceramide/S1P rheostat") determines cell growth and cell death in colon cancer. In the present study, adenoviral overexpression of SphK1 in the liver inhibited tumor growth when colon cancer cells were inoculated after infection. In contrast to AdASM, AdSphK did not exert an inhibitory effect when administered after cell inoculation, which suggests that its inhibitory effect on existing tumors is less than that of AdASM. The observation that AdSphK increased the proliferation of cultured SL4 cells suggests that it decreased the ceramide/S1P ratio in the cancer cells, which may promote their proliferation. In contrast, AdASM might increase the ceramide/S1P ratio, which may inhibit SL4 cell proliferation. We therefore conclude that AdASM, but not AdSphK, may be a useful candidate for gene therapy against metastatic liver tumors of colon cancer.

In *Asm*$^{-/-}$ mice, B16C2M melanoma cells formed small metastatic lesions in the liver (4 of 9, 44.4%) whereas none of the *Asm*$^{+/+}$ mice developed metastases (0 of 11, 0%; Supplemental Figure 7), which suggests that the antitumor effect of ASM is not specific for colon cancer cells. However, use of the *Asm* knockout may have secondary effects due to the severe lipid storage defect in these mice, particularly in macrophages. *Asm*$^{-/-}$ mice are known to have severe immune defects (51, 52) and display severe neurocutaneous disease by 8 weeks of age. Thus, *Asm*$^{-/-}$ mice may have various abnormalities in the liver as a normal pathology. In our study, the livers of *Asm*$^{-/-}$ mice without injection of SL4 cells did not show the nodular appearance. In addition, liver weight of *Asm*$^{-/-}$ mice without injection of SL4 cells was comparable to that of *Asm*$^{+/+}$ mice. Thus, it seems unlikely that the changes are due to normal *Asm*$^{-/-}$ mouse pathology. In addition, besides ASM, ceramide synthesized by the de novo pathway can be involved in TIMP1 regulation. These data do not provide direct evidence that S1P production in hepatocytes recruits macrophages, and experiments using mice with conditional knockout of SphK are also required to confirm the involvement of SphK and S1P in macrophage recruitment and TIMP1 regulation. Moreover, the mechanism by which tumor cells stimulate ASM expression in hepatocytes remains unclear, and there is no direct evidence of a positive correlation between ASM activity in hepatocytes and TIMP1 expression in hMFs; further studies are needed to resolve these uncertainties. In conclusion, we found here that ASM in hepatocytes inhibited tumor growth via S1P formation and subsequent cytotoxic macrophage accumulation. This S1P formation in turn stimulated TIMP1 production by hMFs, leading to tumor suppression. Thus, targeting ASM may represent a new therapeutic strategy for treating liver metastasis of colon cancer.

## Methods

*Animals.* *Asm*$^{-/-}$ mice (C57BL/6 background; ref. 47) were bred for use in this study. *GFP*$^+$ mice (C57BL/6 background), which express EGFP ubiquitously under the CAG promoter (chicken β-actin promoter, rabbit β-globin poly A, CMV-IE enhancer), were obtained from Riken Bio Resource Center. *Timp1*$^{-/-}$ mice (C57BL/6 background) were obtained from Jackson Laboratory. Male Wistar rats and female C57BL/6J wild-type mice were obtained from Japan SLC. *GFP*$^+$*Asm*$^{-/-}$ mice were generated for this study.

*Cell culture.* A red fluorescent protein–expressing mouse colon adenocarcinoma cell line (SL4; Anti-Cancer Japan, Osaka, Japan) was maintained as a monolayer culture in RPMI-1640 (Invitrogen) containing 10% FBS supplemented with penicillin and streptomycin (Invitrogen). Cells were harvested using trypsin and EDTA, washed with PBS, and then resuspended in serum-free RPMI-1640 ($2 \times 10^5$ or $5 \times 10^6$ cells/ml).

*Liver metastasis model.* Female wild-type (C57BL/6J) mice aged 8–10 weeks were divided into 2 groups. After a small incision was made under anesthesia to expose the spleen, 0.1 ml of a viable cell suspension containing $5 \times 10^5$ cells/mouse was injected into the spleen of group 1, and the same suspension containing $2 \times 10^4$ cells/mouse was injected into group 2. Mice were sacrificed on day 7 (group 1) and day 14 (group 2) after cell inoculation. The livers of group 1 were immediately removed, washed in ice-cold PBS, and weighed, after which a part of the dissected liver tissue was frozen in liquid nitrogen. For assessment of liver metastatic tumors in group 2, the intrahepatic tumor was scored as the hepatic replacement area and maximum diameter of tumor, based on examination of 3 nonsequential H&E-stained sections using ImageJ software (NIH). For detection of GFP fluorescence, livers were first perfused in situ with 0.5 mM EGTA containing salt solution to remove peripheral blood cells. The livers were then perfused with 4% paraformaldehyde, fixed with 4% paraformaldehyde for 24 hours, soaked in 15% sucrose in PBS for 12 hours, soaked in 30% sucrose for 24 hours at 4°C under constant agitation, and then embedded in OCT compound to cut sections on a cryostat. The $GFP^+$ area was determined using ImageJ software and shown as a percentage of the total section area.

*Histological analysis.* F4/80, desmin, α-SMA, and TIMP1 were stained with anti-F4/80 (Santa Cruz Biotechnology), anti-desmin (Lab Vision), anti-α-SMA (clone 1A4; Sigma-Aldrich), and anti-TIMP1 (R&D Systems) antibodies, respectively, using Vectastain Elite ABC Kit or M.O.M Immunodetection Kit (Vector Laboratories). Diaminobenzidine tetrahydrochloride was used as peroxidase substrate, and sections were counterstained with hematoxylin. The immunostain-positive area was determined using ImageJ software and shown as a percentage of the total section area. In some experiments, fluorescent dye–labeled secondary antibodies (Alexa Fluor 350 anti-rat for F4/80, Alexa Fluor 488 anti-rabbit for desmin, and Alexa Fluor 594 anti-goat for TIMP1) were used for detection of primary antibodies.

*Depletion of macrophages.* Liposome-encapsulated alendronate (Sigma-Aldrich) was generated as previously reported (53). The alendronate was injected in the mice 4 times: 1 day before cell inoculation and 4, 7, and 10 days after. Liposome-encapsulated PBS was injected into the mice as a control.

*Recombinant adenoviruses.* Mice were infected with 2 adenoviruses ($5 \times 10^8$ pfu/mouse) by intravenous injection 1 day before or 5 days after cell inoculation. Of the 2 adenovirus-5 variants, AdGFP expresses GFP, whereas AdASM expresses both ASM and GFP, because it contains a GFP sequence (27).

*Mass spectrometric (MS) analysis of S1P.* Electrospray ionization MS/MS analysis was performed using a Thermo-Finnigan TSQ 7000 Triple Quadrupole Mass Spectrometer (GenTEch Scientific Inc.) in multiple-reaction monitoring positive ionization mode, as previously reported (54). S1P level was normalized by total protein per sample.

*Macrophage migration assay.* For isolation of peritoneal macrophages, wild-type mice were injected intraperitoneally with cold normal saline. Peritoneal macrophages were purified using MACS Cell Separation Columns with CD11b microbeads (Miltenyi Biotec) from the lavage fluid. The cell migration assay was performed using 24-well transwell plates (5-μm pore size; Costar). The peritoneal macrophages ($1 \times 10^5$ cells) in DMEM containing 1% BSA were loaded into the upper chambers, while the lower chambers were filled with medium with or without 1 μM S1P (Matreya LLC). Cells were incubated for 4 hours, then the migrated macrophages on the underside of the chambers were fixed and stained with Giemsa solution (Wako). Migration was expressed as the number of cells per field.

*Quantitative real-time RT-PCR.* Rat primary liver hMFs were isolated as previously described (25). The cells were cultured in DMEM with 10% FBS on plastic dishes for 4 hours and administered S1P or vehicle (1 μM), and RNA was extracted 0 or 72 hours after S1P stimulation. The RNeasy and DNase Kits (Qiagen) was used for RNA extraction from liver tissue and cultured cells, and the High-Capacity cDNA Reverse Transcription Kit (Applied Biosystems) was used for reverse transcription. Quantitative real-time RT-PCR was performed using the SYBR Premix Ex Taq (Takara) for *Timp1* (forward, TGGGGAACCCATGAATTTAG; reverse, TCTGGCATCCTCTTGTTGC) and probe and primer sets (Applied Biosystems) for 18S with LightCycler 480 (Roche Applied Science). The changes were normalized based on 18S rRNA values.

*Statistics.* Data are expressed as mean ± SD of data collected from 5 independent experiments. Data between groups were analyzed by 2-tailed Student's *t* test. A *P* value less than 0.05 was considered significant.

*Study approval.* All experiments were conducted in accordance with the institutional guidelines of Gifu University and were approved by the animal research committee and the committee on living modified organisms of Gifu University.

## Acknowledgments

This work was supported by grants from the Takeda Science Foundation, the Kondou Kinen Medical Foundation, the Kurozumi Medical Foundation, the Yasuda Medical Foundation, and the Senshin Medical Research Foundation and by Grants-in-Aid for Scientific Research from the Ministry of Education, Science, Sports, and Culture of Japan (23790787, 24890081, and 22590726). We thank Jacek Bielawski for conducting the sphingolipid measurement and Yoshiko Banno for performing the measurement of ASM activity. B16C2M cells were provided by the Cell Resource Center for Biomedical Research, Institute of Development, Aging and Cancer, Tohoku University (Sendai, Japan).

Received for publication June 12, 2012, and accepted in revised form November 13, 2012.

Address correspondence to: Yosuke Osawa, Department of Pharmacology, Gifu University Graduate School of Medicine, 1-1 Yanagido Gifu 501-1194, Japan. Phone: 81.58.230.6217; Fax: 81.58.230.6218; E-mail: osawa-gif@umin.ac.jp.

1. Smith EL, Schuchman EH. The unexpected role of acid sphingomyelinase in cell death and the pathophysiology of common diseases. *FASEB J.* 2008; 22(10):3419–3431.
2. Jenkins RW, Canals D, Hannun YA. Roles and regulation of secretory and lysosomal acid sphingomyelinase. *Cell Signal.* 2009;21(6):836–846.
3. Hannun YA. Functions of ceramide in coordinating cellular responses to stress. *Science.* 1996; 274(5294):1855–1859.
4. Furuya H, Shimizu Y, Kawamori T. Sphingolipids in cancer. *Cancer Metastasis Rev.* 2011;30(3–4):567–576.
5. Nemoto S, et al. Sphingosine kinase isoforms regulate oxaliplatin sensitivity of human colon cancer cells through ceramide accumulation and Akt activation. *J Biol Chem.* 2009;284(16):10422–10432.
6. Coussens LM, Werb Z. Inflammation and cancer. *Nature.* 2002;420(6917):860–867.
7. Hagemann T, Biswas SK, Lawrence T, Sica A, Lewis CE. Regulation of macrophage function in tumors: the multifaceted role of NF-κB. *Blood.* 2009; 113(14):3139–3146.
8. Condeelis J, Pollard JW. Macrophages: obligate partners for tumor cell migration, invasion, and metastasis. *Cell.* 2006;124(2):263–266.
9. Mantovani A, Allavena P, Sica A, Balkwill F. Cancer-related inflammation. *Nature.* 2008; 454(7203):436–444.
10. Bingle L, Brown NJ, Lewis CE. The role of tumour-associated macrophages in tumour progression: implications for new anticancer therapies. *J Pathol.* 2002;196(3):254–265.
11. Zhou Q, et al. The density of macrophages in the invasive front is inversely correlated to liver metastasis in colon cancer. *J Transl Med.* 2010;8:13.
12. Forssell J, et al. High macrophage infiltration along the tumor front correlates with improved survival in colon cancer. *Clin Cancer Res.* 2007; 13(5):1472–1479.
13. Mosser DM, Edwards JP. Exploring the full spectrum of macrophage activation. *Nat Rev Immunol.* 2008; 8(12):958–969.
14. Balkwill F, Charles KA, Mantovani A. Smoldering and polarized inflammation in the initiation and promotion of malignant disease. *Cancer Cell.* 2005; 7(3):211–217.
15. Ma J, et al. The M1 form of tumor-associated macrophages in non-small cell lung cancer is posi-

tively associated with survival time. *BMC Cancer.* 2010;10:112.
16. Keul P, et al. Sphingosine-1-phosphate receptor 3 promotes recruitment of monocyte/macrophages in inflammation and atherosclerosis. *Circ Res.* 2011; 108(3):314–323.
17. Rivera J, Proia RL, Olivera A. The alliance of sphingosine-1-phosphate and its receptors in immunity. *Nat Rev Immunol.* 2008;8(10):753–763.
18. Weigert A, et al. Tumor cell apoptosis polarizes macrophages role of sphingosine-1-phosphate. *Mol Biol Cell.* 2007;18(10):3810–3819.
19. Keul P, et al. The sphingosine-1-phosphate analogue FTY720 reduces atherosclerosis in apolipoprotein E-deficient mice. *Arterioscler Thromb Vasc Biol.* 2007;27(3):607–613.
20. Wagenaar-Miller RA, Gorden L, Matrisian LM. Matrix metalloproteinases in colorectal cancer: is it worth talking about? *Cancer Metastasis Rev.* 2004; 23(1–2):119–135.
21. Elezkurtaj S, et al. Adenovirus-mediated overexpression of tissue inhibitor of metalloproteinases-1 in the liver: efficient protection against T-cell lymphoma and colon carcinoma metastasis. *J Gene Med.* 2004;6(11):1228–1237.
22. Martin DC, Ruther U, Sanchez-Sweatman OH, Orr FW, Khokha R. Inhibition of SV40 T antigen-induced hepatocellular carcinoma in TIMP-1 transgenic mice. *Oncogene.* 1996;13(3):569–576.
23. Kruger A, Fata JE, Khokha R. Altered tumor growth and metastasis of a T-cell lymphoma in Timp-1 transgenic mice. *Blood.* 1997;90(5):1993–2000.
24. Jiang Y, Goldberg ID, Shi YE. Complex roles of tissue inhibitors of metalloproteinases in cancer. *Oncogene.* 2002;21(14):2245–2252.
25. Osawa Y, Hannun YA, Proia RL, Brenner DA. Roles of AKT and sphingosine kinase in the antiapoptotic effects of bile duct ligation in mouse liver. *Hepatology.* 2005;42(6):1320–1328.
26. Li C, et al. Sphingosine 1-phosphate (S1P)/S1P receptors are involved in human liver fibrosis by action on hepatic myofibroblasts motility. *J Hepatol.* 2011;54(6):1205–1213.
27. Osawa Y, et al. Acid sphingomyelinase regulates glucose and lipid metabolism in hepatocytes through AKT activation and AMP-activated protein kinase suppression. *FASEB J.* 2011;25(4):1133–1144.
28. Kan Z, et al. In vivo microscopy of hepatic metastases: dynamic observation of tumor cell invasion and interaction with Kupffer cells. *Hepatology.* 1995;21(2):487–494.
29. Klimp AH, de Vries EG, Scherphof GL, Daemen T. A potential role of macrophage activation in the treatment of cancer. *Crit Rev Oncol Hematol.* 2002; 44(2):143–161.
30. Caignard A, et al. Role of macrophage in the defense against intestinal cancers. *Comp Immunol Microbiol Infect Dis.* 1985;8(2):147–157.
31. Bayon LG, et al. Role of Kupffer cells in arresting circulating tumor cells and controlling metastatic growth in the liver. *Hepatology.* 1996;23(5):1224–1231.
32. Holten-Andersen MN, et al. Localization of tissue inhibitor of metalloproteinases 1 (TIMP-1) in human colorectal adenoma and adenocarcinoma. *Int J Cancer.* 2005;113(2):198–206.
33. Granado MH, et al. Ceramide 1-phosphate (C1P) promotes cell migration Involvement of a specific C1P receptor. *Cell Signal.* 2009;21(3):405–412.
34. Schulze-Krebs A, et al. Hepatitis C virus-replicating hepatocytes induce fibrogenic activation of hepatic stellate cells. *Gastroenterology.* 2005;129(1):246–258.
35. Schissel SL, Keesler GA, Schuchman EH, Williams KJ, Tabas I. The cellular trafficking and zinc dependence of secretory and lysosomal sphingomyelinase, two products of the acid sphingomyelinase gene. *J Biol Chem.* 1998;273(29):18250–18259.
36. Spiegel S, Milstien S. The outs and the ins of sphingosine-1-phosphate in immunity. *Nat Rev Immunol.* 2011;11(6):403–415.
37. Osawa Y, et al. TNF-α-induced sphingosine 1-phosphate inhibits apoptosis through a phosphatidylinositol 3-kinase/Akt pathway in human hepatocytes. *J Immunol.* 2001;167(1):173–180.
38. Sica A, Bronte V. Altered macrophage differentiation and immune dysfunction in tumor development. *J Clin Invest.* 2007;117(5):1155–1166.
39. Dunn GP, Bruce AT, Ikeda H, Old LJ, Schreiber RD. Cancer immunoediting: from immunosurveillance to tumor escape. *Nat Immunol.* 2002;3(11):991–998.
40. Morimoto-Tomita M, Ohashi Y, Matsubara A, Tsuiji M, Irimura T. Mouse colon carcinoma cells established for high incidence of experimental hepatic metastasis exhibit accelerated and anchorage-independent growth. *Clin Exp Metastasis.* 2005; 22(6):513–521.
41. De Wever O, et al. Tenascin-C and SF/HGF produced by myofibroblasts in vitro provide convergent pro-invasive signals to human colon cancer cells through RhoA and Rac. *FASEB J.* 2004; 18(9):1016–1018.
42. Tsujino T, et al. Stromal myofibroblasts predict disease recurrence for colorectal cancer. *Clin Cancer Res.* 2007;13(7):2082–2090.
43. Barsky SH, Gopalakrishna R. Increased invasion and spontaneous metastasis of BL6 melanoma with inhibition of the desmoplastic response in C57 BL/6 mice. *Cancer Res.* 1987;47(6):1663–1667.
44. Peyrol S, et al. Lysyl oxidase gene expression in the stromal reaction to in situ and invasive ductal breast carcinoma. *Am J Pathol.* 1997;150(2):497–507.
45. Moskovits N, Kalinkovich A, Bar J, Lapidot T, Oren M. p53 Attenuates cancer cell migration and invasion through repression of SDF-1/CXCL12 expression in stromal fibroblasts. *Cancer Res.* 2006; 66(22):10671–10676.
46. Pettus BJ, Chalfant CE, Hannun YA. Ceramide in apoptosis: an overview and current perspectives. *Biochim Biophys Acta.* 2002;1585(2–3):114–125.
47. Osawa Y, et al. Roles for C16-ceramide and sphingosine 1-phosphate in regulating hepatocyte apoptosis in response to tumor necrosis factor-α. *J Biol Chem.* 2005;280(30):27879–27887.
48. Spiegel S, Milstien S. Sphingosine-1-phosphate: an enigmatic signalling lipid. *Nat Rev Mol Cell Biol.* 2003;4(5):397–407.
49. Kawamori T, et al. Role for sphingosine kinase 1 in colon carcinogenesis. *FASEB J.* 2009;23(2):405–414.
50. Selzner M, et al. Induction of apoptotic cell death and prevention of tumor growth by ceramide analogues in metastatic human colon cancer. *Cancer Res.* 2001;61(3):1233–1240.
51. Kuemmel TA, Thiele J, Schroeder R, Stoffel W. Pathology of visceral organs and bone marrow in an acid sphingomyelinase deficient knock-out mouse line, mimicking human Niemann-Pick disease type A. A light and electron microscopic study. *Pathol Res Pract.* 1997;193(10):663–671.
52. Horinouchi K, et al. Acid sphingomyelinase deficient mice: a model of types A and B Niemann-Pick disease. *Nat Genet.* 1995;10(3):288–293.
53. Osawa Y, et al. Role of acid sphingomyelinase of Kupffer cells in cholestatic liver injury in mice. *Hepatology.* 2010;51(1):237–245.
54. Pettus BJ, et al. The sphingosine kinase 1/sphingosine-1-phosphate pathway mediates COX-2 induction and PGE2 production in response to TNF-α. *FASEB J.* 2003;17(11):1411–1421.

JOURNAL OF VIRAL HEPATITIS JVH

*Journal of Viral Hepatitis*, 2013, **20**, 350–357 doi:10.1111/jvh.12031

# Hepatocyte destruction with enhanced collagen synthesis: characteristic feature of chronic hepatitis C patients on haemodialysis

M. Ue,[1] N. Ikebe,[2] K. Munekage,[1] T. Ochi,[1] A. Hirose,[1] H. Kataoka,[3] S. Fujimoto,[4] K. Kikuchi,[5] Y. Okuhara,[3] M. Ono[1] and T. Saibara[1] [1]*Department of Gastroenterology and Hepatology, Kochi Medical School, Nankoku, Kochi, Japan;* [2]*Department of Surgery, Kochi Takasu Hospital, Kochi, Japan;* [3]*Center of Medical Information Science, Kochi Medical School, Nankoku, Kochi, Japan;* [4]*Department of Endocrinology, Metabolism, and Nephrology, Kochi Medical School, Kochi, Japan; and* [5]*Shimoochiai Clinic, Tokyo, Japan*

*Received August 2012; accepted for publication October 2012*

SUMMARY. Hepatitis C virus (HCV) infection is frequent among patients with end-stage renal disease on haemodialysis and is considered to be an independent risk factor for mortality in this setting. However, only a few of these patients are treated with anti-hepatitis virus treatment before the development of end-stage renal disease. Recent guidelines recommend identification of patients with good prognoses who are in need of interferon treatment, but we know little of patients who must be treated urgently. Ninety-eight patients on haemodialysis (48 anti-HCV-positive and 50 anti-HCV-negative patients) were enrolled in this study; HCV RNA was detected in 43 anti-HCV-positive patients. Univariate analysis and multivariate regression analysis were applied to identify variables independently associated with persistent HCV infection. Seven variables were proven to be associated with persistent HCV infection. Among them, type IV collagen 7S and N-terminal propeptide of type III procollagen (P-III-P) were defined as independent variables useful in distinguishing HCV RNA-positive patients from HCV RNA-negative patients with 0.91 sensitivity, 0.91 specificity, 0.89 positive predictive value and 0.93 negative predictive value. Our observations suggest that hepatocyte destruction with enhanced liver fibrosis is a characteristic clinical feature of persistent HCV infection. Type IV collagen 7S of $\geq 5$ ng/mL and/or P-III-P of $\geq 5$ U/mL would be useful markers to identify patients in need of interferon treatment, which supports the idea of the Kidney Disease: Improving Global Outcomes guidelines that a good prognosis in patients with HCV infection on haemodialysis should prompt consideration for IFN treatment when applicable.

*Keywords:* chronic hepatitis C, collagen synthesis, haemodialysis, IFN therapy.

## INTRODUCTION

Chronic hepatitis C (CH-C) is a very important life-threatening disease in the general population. However, it has become an easily manageable liver disease in industrialized countries because treatment with interferon (IFN) is available and effective. However, CH-C was regarded to be neither a life-threatening complication nor a risk factor for decreased quality of life among patients with end-stage renal disease on haemodialysis (HD) for the long term. The reason for this is that the life expectancy of patients undergoing HD was rather short because of frequent complications of atherosclerotic cardiovascular disease. Therefore, IFN treatment has been administered to only a few patients with both CH-C and end-stage renal disease, and the inclusion criteria of interferon treatment for patients undergoing HD have not yet been clarified.

Recent progress in the quality of HD procedures and the preventive protocol for atherosclerosis has enabled an increase in the 10-year survival among patients undergoing HD, while 10% of patients with end-stage renal disease suffer from CH-C [1–7]. This frequency is much higher than that in the general population, and the number of patients with CH-C undergoing long-term HD is rapidly increasing [2,8,9]. We assume that the mortality rate

Abbreviations: ALT, alanine aminotransferase; APRI, AST to platelet count ratio index; AST, aspartate aminotransferase; CH-C, chronic hepatitis C; HA, hyaluronic acid; HCV, hepatitis C virus; HD, haemodialysis; IFN, interferon; KDIGO, Kidney Disease: Improving Global Outcomes; P-III-P, N-terminal propeptide of type III procollagen.

Correspondence: Masafumi Ono, MD, PhD, Department of Gastroenterology and Hepatology, Kohasu, Oko-cho, Nankoku, Kochi 783-8505, Japan.
E-mail: onom@kochi-u.ac.jp

caused by liver cirrhosis and/or hepatocellular carcinoma may gradually increase worldwide, including in Japan, in the near future as observed in patients not undergoing HD [2,8,9]. With this background, Kidney Disease: Improving Global Outcomes (KDIGO) published their guidelines for patients with CH-C undergoing HD. The society recommended defining candidates for anti-hepatitis virus treatment including IFN as relatively young patients with a good prognosis and life expectancy of >5 years and without cardiovascular disease [10]. The Japanese Society for Dialysis Therapy also published guidelines for the treatment of patients with CH-C undergoing HD. The society noted that (i) the prevalence of CH-C is very high among patients undergoing HD, (ii) the prognosis of patients undergoing HD with HCV infection was worse than that of patients without HCV infection and (iii) life expectancy could be improved by preventing HCV infection or treating CH-C [11].

Patients with CH-C undergoing HD are in need of treatment, but we know little of which patients should be treated urgently and why they should be treated extensively. In this study, we characterized clinical features of patients with CH-C undergoing HD using biochemical markers including aspartate aminotransferase (AST), alanine aminotransferase (ALT) and so-called liver fibrosis markers such as serum levels of N-terminal propeptide of type III procollagen (P-III-P), type IV collagen 7S and hyaluronic acid (HA) [12–14].

## PATIENTS AND METHODS

### *Patients*

Ninety-eight patients undergoing HD at Kochi Takasu Hospital (48 patients positive for anti-HCV antibody and 50 negative for anti-HCV antibody) were enrolled in this study. Informed consent was obtained at the time of laboratory testing. This study was conducted in conformance with the Helsinki Declaration. Any patients with hepatitis B surface antigen, alcohol intake of >20 g per day or evidence of hepatocellular carcinoma or other aetiologies of liver disease including autoimmune hepatitis, drug-induced liver disease, primary biliary cirrhosis, biliary obstruction, haemochromatosis or Wilson's disease were excluded from this study. Forty-eight anti-HCV patients undergoing HD were divided into two groups: 43 were positive for HCV RNA (Group 1) and 5 were negative for HCV RNA (Group 2). Fifty anti-HCV-negative patients undergoing HD were also enrolled as the study controls (Group 3).

### *Laboratory evaluations*

Venous blood samples were obtained immediately before starting HD. Laboratory evaluation in all patients included a blood cell count, and measurements of AST, ALT, albumin, HA (reference range, <50 ng/mL; LPIA-ACE HA; Mitsubishi Chemical Medience Co., Tokyo, Japan), P-III-P (reference range, 0.3–0.8 U/mL; Ryagnost P-III-P; Cisbio International, Bagnols/Ceze, France) and type IV collagen 7S (reference range, <6 ng/mL; Type IV collagen 7S kit; Mitsubishi Chemical Medience Co., Tokyo, Japan) were measured using a standard automated analyser in the clinical laboratory of Kochi Takasu Hospital.

### *Virological assays*

Anti-HCV was detected by third-generation enzyme immunoassay systems (Abbott Laboratories Diagnostic Division, Abbott Park, IL,USA). HCV RNA was assessed by TaqMan PCR assays (Roche Diagnostics Systems, Branchburg, NJ, USA). Hepatitis B surface antigen was detected by automated chemiluminescence enzyme immunoassay systems (Abbott Laboratories Diagnostic Division, Abbott Park, IL, USA).

### *Aspartate aminotransferase (AST) to platelet count ratio index*

The ratio of AST (IU/L) to platelet count ($\times 10^3/\mu L$) in peripheral blood AST to platelet count ratio index (APRI) was used as an indicator of advanced liver fibrosis where an APRI of <0.40 has been proposed to accurately identify 93% of patients with mild liver fibrosis (stage 0 or 1) [1,15].

### *Statistical analysis*

Continuous variables were expressed as mean ± standard deviation. The Mann–Whitney *U*-test, Student's *t*-test and the chi-square test were used when applicable. Laboratory data were applied to univariate analysis to define variables that were significantly different between patients undergoing HD with and without CH-C ($P < 0.05$). Those variables were then further applied to multivariate analysis to identify variables that independently contributed to the prediction of patients undergoing HD with CH-C. To assess the accuracy of detection of patients undergoing HD with CH-C, receiver operating characteristic (ROC) curves were constructed using variables, for example serum levels of P-III-P and type IV collagen 7S. The Youden index was used to identify the optimal cut-off points. The sensitivity, specificity, positive predictive value and negative predictive value were calculated for the two cut-off values proposed by Sterling *et al.* [16]. Differences were considered statistically significant for *P* values of <0.05.

## RESULTS

### *Univariate analysis between patients undergoing haemodialysis (HD) with and without CH-C*

There were no significant differences in age or gender among Groups 1, 2 and 3 (Table 1). In univariate analysis

**Table 1** Univariate analysis between patients undergoing haemodialysis (HD) with and without chronic hepatitis C (CH-C)

| | Group 1 ($n$ = 43) HCV-RNA(+) | Group 2 ($n$ = 5) HCV-RNA(−) HCV-Ab(+) | Group 3 ($n$ = 50) HCV-RNA(−) HCV-Ab(−) | Group 2 + 3 ($n$ = 55) HCV-RNA(-) | $P$ value Group 1 *vs* Group 2 + 3 |
|---|---|---|---|---|---|
| Age (year) | 66.7 ± 8.2 | 76.0 ± 8.2 | 67.8 ± 10.0 | 68.5 ± 10.1 | 0.35 |
| Gender (F/M) | 16/27 | 2/3 | 24/26 | 26/29 | 0.32 |
| AST (IU/L) | 22.5 ± 11.3 | 15.2 ± 2.8 | 16.0 ± 5.5 | 16.0 ± 5.3 | <0.001 |
| ALT (IU/L) | 22.8 ± 18.3 | 10.7 ± 2.9 | 13.2 ± 1.7 | 10 ± 4.6 | <0.001 |
| Albumin (g/dL) | 3.5 ± 0.5 | 3.5 ± 0.3 | 3.7 ± 0.2 | 3.7 ± 0.3 | <0.05 |
| PLT ($\times 10^4/mm^3$) | 15.1 ± 6.2 | 15.9 ± 5.9 | 19.0 ± 6.2 | 18.9 ± 6.2 | <0.005 |
| HA (ng/mL) | 843.8 ± 1548.1 | 281.4 ± 166.0 | 371.8 ± 460.1 | 363.6 ± 441.4 | <0.05 |
| IV col.7S (ng/mL) | 6.1 ± 1.6 | 4.6 ± 0.8 | 4.3 ± 0.9 | 4.4 ± 0.9 | <0.0001 |
| P-III-P (U/m) | 5.2 ± 2.4 | 3.1 ± 1.5 | 2.8 ± 0.9 | 2.7 ± 0.9 | <0.0001 |

There were no significant differences in age or gender among Groups 1, 2 and 3. In univariate analysis between Group 1 and Group 2 + 3, seven variables (serum levels of AST ($P < 0.001$), ALT ($P < 0.001$), HA ($P < 0.05$), type IV collagen 7S ($P < 0.0001$) and P-III-P ($P < 0.0001$) in Group 1 were significantly higher than those in Group 2 + 3. Platelet counts ($P < 0.005$) and serum albumin ($P < 0.05$) in Group 1 were significantly lower than those in Group 2 + 3.
Group 1: (patients with CH-C undergoing HD), Group 2 + 3 (patients without CH-C undergoing HD).

between Group 1 (patients undergoing with CH-C) and Group 2 + 3 (patients undergoing without CH-C), seven variables were defined as significantly different: serum levels of AST ($P < 0.001$), ALT ($P < 0.001$), HA ($P < 0.05$), type IV collagen 7S ($P < 0.0001$) and P-III-P ($P < 0.0001$) in Group 1 were significantly higher than those in Group 2 + 3. Platelet counts ($P < 0.005$) and serum albumin ($P < 0.05$) in Group 1 were significantly lower than those in Group 2 + 3.

### *Multivariate analysis between patients undergoing haemodialysis (HD) with and without chronic hepatitis C (CH-C)*

A binomial regression model using these seven continuous variables was applied to evaluate the key factors involved in distinguishing Group 1 from Group 2 + 3 (Table 1). Serum levels of type IV collagen 7S ($P < 0.001$), P-III-P ($P < 0.001$) and ALT ($P < 0.005$) contributed much to independently distinguish Group 1 from Group 2 + 3 (Table 2). Because the ALT level is notably affected by the serum vitamin B6 level [17], serum levels of type IV collagen 7S and P-III-P were further chosen for binomial regression model analysis; Fig. 1a,b confirm how these two factors work well in the distinction.

### *Receiver operating characteristic (ROC) curve analysis*

Receiver operating characteristic (ROC) curves were created using type IV collagen 7S and P-III-P to verify the usefulness in this distinction (Fig. 2). The area under the ROC curve was revealed to be as high as 0.90 when Akaike's information criterion was 70.1. When the Youden index was used to determine the optimal cut-off value using type IV collagen 7S in combination with P-III-P for distinguishing Group 1 from Group 2 + 3, 0.45 was shown to be optimal with a sensitivity of 0.84, specificity of 0.91, positive predictive value of 0.85 and negative predictive value of 0.92.

**Table 2** Multivariate analysis between patients undergoing haemodialysis (HD) with and without chronic hepatitis C (CH-C). (a) Binomial regression model using these seven continuous variables was applied to evaluate the key factors involved in distinguishing Group 1 from Group 2 + 3. Serum levels of type IV collagen 7S ($P < 0.001$), P-III-P ($P < 0.001$) and ALT ($P < 0.005$) greatly contributed to independently distinguishing Group 1 from Group 2 + 3. (b) Serum levels of type IV collagen 7S ($P < 0.0005$) and P-III-P ($P < 0.0001$) were further chosen for binomial regression model analysis

| | $\beta$ | SE ($\beta$) | Z value | $P$ value |
|---|---|---|---|---|
| (a) | | | | |
| IVcol.7S (ng/mL) | 1.26 | 0.37 | 3.41 | <0.001 |
| P-III-P(U/mL) | 1.03 | 0.30 | 3.45 | <0.001 |
| ALT (IU/L) | 0.24 | 0.08 | 2.93 | <0.005 |
| Alb (g/dL) | −2.03 | 1.12 | 1.82 | 0.069 |
| (b) | | | | |
| IVcol.7S (ng/mL) | 0.91 | 0.25 | 3.68 | <0.0005 |
| P-III-P(U/mL) | 1.29 | 0.33 | 3.95 | <0.0001 |

### *Plot analysis*

Plot analysis revealed another possible way to distinguish these two groups with a sensitivity of 0.91, specificity of

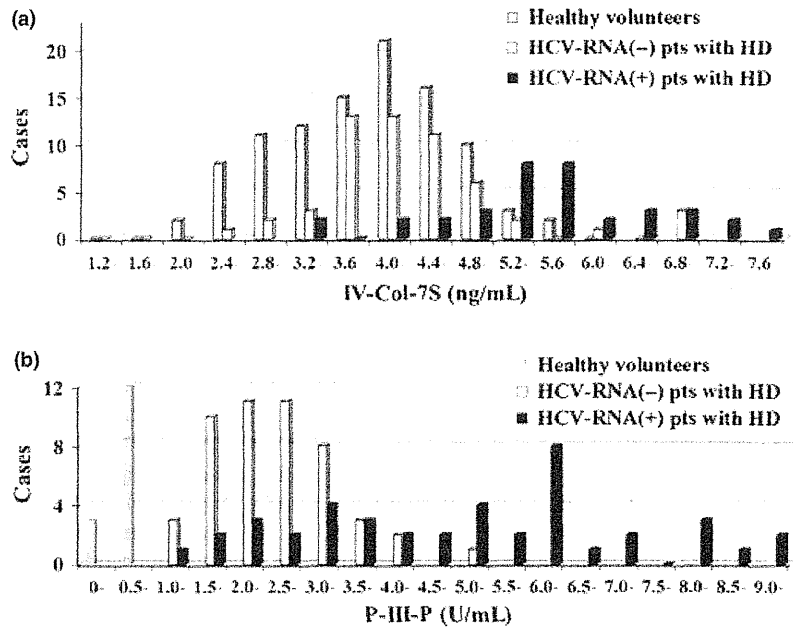


**Fig. 1** Distribution of patients undergoing HD and healthy volunteers in terms of (a) type IV collagen 7S and (b) P-III-P. (a) The distribution of patients without CH-C undergoing HD in terms of type IV collagen 7S was quite similar to that of healthy volunteers. In contrast, the distribution of patients with CH-C undergoing HD in terms of type IV collagen 7S was remarkably higher than that of patients without CH-C undergoing HD. (b) The distribution of patients without CH-C undergoing HD in terms of P-III-P was higher than that of healthy volunteers. In addition, the distribution of patients with CH-C undergoing HD in terms of P-III-P was significantly higher than that of patients without CH-C undergoing HD.

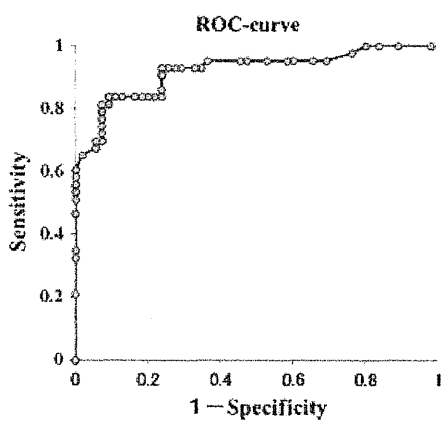


**Fig. 2** Receiver operating characteristic (ROC) curve analysis. ROC curves were created using type IV collagen 7S and P-III-P to verify the usefulness in this distinction. The area under the receiver operating characteristic curve was revealed to be as high as 0.90 when Akaike's information criterion was 70.1. When the Youden index was used to determine the optimal cut-off value using type IV collagen 7S in combination with P-III-P for distinguishing Group 1 from Group 2 + 3, 0.45 was shown to be optimal with a sensitivity of 0.84, specificity of 0.91, positive predictive value of 0.85 and negative predictive value of 0.92.

0.91, positive predictive value of 0.89 and negative predictive value of 0.93. Indeed, the majority of patients with CH-C were distributed in the area of either type IV collagen 7S of $\geq$ 5 ng/mL or P-III-P of $\geq$ 5 U/mL, while those without CH-C (Groups 2 and 3) remained in the area of type IV collagen 7S of <5 ng/mL and P-III-P of <5 U/mL (Fig. 3a). Thus, the odds ratio was calculated to be as high as 70.3 in predicting patients undergoing with CH-C (95% confidence intervals, 19.0–257.2).

### *AST to platelet count ratio index (APRI)*

We next investigated the relationship between these fibrosis markers (type IV collagen 7S and P-III-P) and the degree of advanced fibrosis. APRI was originally designed to predict advanced liver fibrosis in patients with CH-C not undergoing HD [1]. Schiavon LL *et al.* reported that APRI was also useful as a noninvasive marker for the evaluation of advanced hepatic fibrosis (APRI $\geq$ 0.40) in patients with CH-C undergoing HD [15]. Therefore, we evaluated advanced hepatic fibrosis by APRI and compared our results with type IV collagen 7S and P-III-P in patients with CH-C (Group 1; Fig. 3b). However, no relationship between APRI of $\geq$0.40 and these two fibrosis markers was found. We then compared platelet counts in the patients with type IV collagen 7S and P-III-P levels other than <5 ng/mL and <5 U/mL, respectively (Fig. 4). The average platelet count in the patients with an APRI of $\geq$0.40 was remarkably lower ($12.0 \pm 4.2 \times 10^4/\mu L$) than that in the patients with an APRI of <0.40 ($18.6 \pm 5.8 \times 10^4/\mu L$, $P < 0.001$). In addition, platelet counts in many patients with an APRI of $\geq$0.40 were $>10 \times 10^4/\mu L$, which indicated severe advanced hepatic fibrosis.

## DISCUSSION

Barril *et al.* [18] reported that the progression time to cirrhosis can be much shorter in patients with CH-C undergoing HD than in those not undergoing HD. On the contrary,

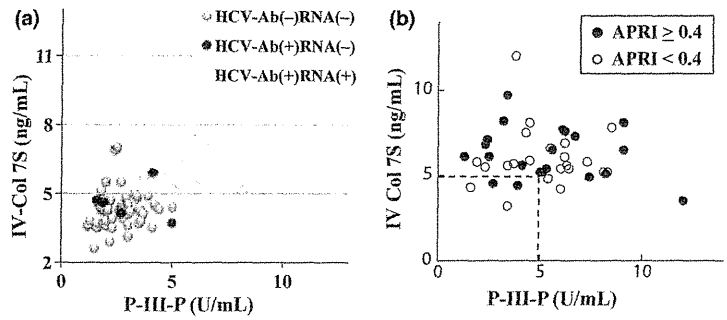


**Fig. 3** Relationship between type IV collagen 7S and P-III-P values. (a) Relationship between type IV collagen 7S and P-III-P values among HCV-Ab (+) RNA (+) (Group 1: open circle), HCV-Ab (+) RNA (−) (Group 2: closed circle) and HCV-Ab (−) RNA (−) (Group 3: grey circle). Most patients in Group 1 (patients with CH-C) were outside the ranges of type IV collagen 7S of <5 ng/mL and P-III-P of <5 U/mL. In contrast, most patients in Group 2 + 3 were within the ranges of type IV collagen 7S of <5 ng/mL and P-III-P of <5 U/mL. (b) Relationships among type IV collagen 7S, P-III-P and APRI in patients with CH-C (Group 1). There were no differences in either type IV collagen 7S or P-III-P between patients with CH-C (Group 1) with an APRI of ≥0.4 and those with and APRI of <0.4 (APRI: AST to platelet count ratio index).

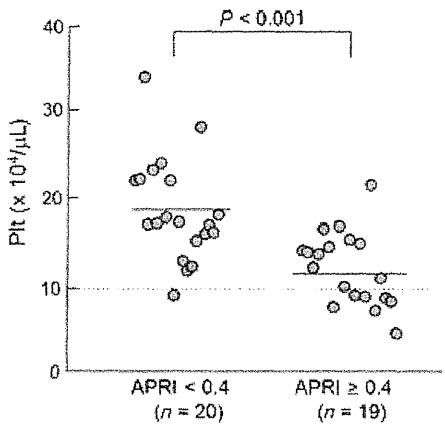


**Fig. 4** Platelet counts in the patients outside the range of type IV collagen 7S of <5 ng/mL and P-III-P of <5 U/mL. The patients with CH-C with an APRI of ≥0.40 ($n$ = 19) had significantly lower platelet counts (12.0 ± 4.2 × $10^4/\mu L$) than those with an APRI of <0.40 ($n$ = 20, 18.6 ± 5.8 × $10^4/\mu L$, $P$ < 0.001). The many patients with an APRI of ≥0.40 had lower platelet counts (>10 × $10^4/\mu L$) compared with the patients with an APRI of <0.40.

others suggest that patients with CH-C undergoing HD present a lower degree of inflammatory activity and a lower stage of liver fibrosis compared with patients with CH-C not undergoing HD [19–21]. Thus, whether the natural clinical course of liver fibrosis in patients with CH-C undergoing HD is more progressive than that observed in patients with CH-C not undergoing HD is controversial [19–23]. Indeed, the effects of end-stage renal disease and HD on the progression of CH-C have remained largely unknown until today. Therefore, the most important elucidation of this study is whether or not the natural clinical course of liver fibrosis in patients with CH-C undergoing HD is more progressive.

Hepatocyte destruction with liver fibrosis is the most characteristic pathological feature of chronic hepatitis. Liver biopsy is the most reliable procedure to estimate the degree of hepatitis and the stage of liver fibrosis, but liver biopsy is not indicated in these cases because patients undergoing HD are at a serious risk of bleeding [22,24,25]. For this reason, we evaluated the factors that efficiently distinguish patients with CH-C undergoing HD (Group 1) from those without CH-C (Group 2 + 3) in this study using a binomial regression model. Univariate analysis revealed seven factors that were useful for distinguishing these two groups, and multivariate regression analysis has proven that three of the seven factors (serum levels of type IV collagen 7S, P-III-P and ALT) were independent factors for the distinction with very high sensitivity and specificity when other aetiologies of chronic liver disease, such as alcoholic liver disease, were excluded ($P$ < 0.005).

The serum level of ALT, an excellent marker of hepatocyte destruction, remained within the reference range in most patients with CH-C undergoing HD as previously reported [8,26–28], but it was significantly higher in patients with CH-C undergoing HD than in patients without CH-C undergoing HD. Liver fibrosis consists of the deposition of fibrillar extracellular matrix components in response to viral infections and other pathogenic factors. Serum levels of type IV collagen 7S and P-III-P, which are tightly associated with this deposition process, are markers of enhanced collagen synthesis at the site of hepatocyte destruction [29–31]. Their serum levels, which are determined by the balance between their production and degradation, were significantly higher in most patients with CH-C undergoing HD

than in patients without CH-C undergoing HD. Taken together, these observations strongly suggest that most patients with CH-C undergoing HD have enhanced hepatocyte destruction with collagen synthesis in the liver when compared with those without CH-C.

The odds ratio assessed by the chi-square test was as high as 70.3 in defining patients with CH-C undergoing HD because both positive and negative predictive values were very high in this case. ROC curves using serum levels of type IV collagen 7S and P-III-P further confirmed this observation. On the other hand, plot analysis revealed that serum levels of type IV collagen 7S of $\geq 5$ ng/mL and/or P-III-P of $\geq 5$ U/mL also distinguished patients with CH-C undergoing HD from those without CH-C very well. All of these results support the guidelines stating why most patients with CH-C undergoing HD, who are relatively young and have a life expectancy of >5 years and do not have cardiovascular disease, should be considered as candidates for anti-hepatitis virus treatment including IFN [10].

Patients with CH-C have been treated extensively, but few patients with CH-C undergoing HD have been regarded as candidates for IFN treatment. However, liver disease has become one of the leading causes of death in long-term renal transplant survivors [2,3], and pretransplant IFN treatment for patients undergoing renal transplantation with CH-C attenuated chronic allograft nephropathy [32] and prevented the development of diabetes mellitus and HCV-associated glomerulonephritis in renal allografts [33,34]. Thus, patients with CH-C and advanced liver fibrosis are assumed to be candidates in urgent need of anti-hepatitis virus treatment, although the frequency of advanced liver fibrosis and liver cirrhosis ranges from 5% to 32% at most [18–21,35–38].

The frequency is rather low, and our next question is how to define patients with CH-C and advanced liver fibrosis (stages 2, 3 and 4). We herein propose the use of the APRI, because AST and the platelet count in peripheral blood are noninvasive, inexpensive tests available anywhere in the world [15]. This index was introduced in patients with CH-C undergoing HD to distinguish those with advanced liver fibrosis (stages 2, 3 and 4) from those with mild liver fibrosis (stages 0 and 1) [1]. Patients with an APRI of <0.40 reportedly comprise 93% of patients with liver fibrosis stage 0 or 1 and 7% of those with liver fibrosis stage 2 [1,15]. The average APRI in our patients with CH-C undergoing HD (Group 1) was $0.45 \pm 0.28$, and an APRI of $\geq 0.40$, which indicated advanced liver fibrosis, was observed in 21 of 43 patients with CH-C undergoing HD. The result in Fig. 3 indicates that APRI was not always related to the type IV collagen 7S or P-III-P levels in patients with CH-C undergoing HD (Group 1). According to our results mentioned above, the patients with type IV collagen 7S and P-III-P levels of <5 ng/mL and <5 U/mL, respectively, should be considered for IFN treatment. We next examined the platelet counts in advanced liver fibrosis (APRI $\geq$ 0.40) and mild liver fibrosis (APRI < 0.40) (Fig. 4). The average platelet count in the patients with an APRI of $\geq 0.4$ was remarkably lower ($12.0 \pm 4.2 \times 10^4/\mu L$) than that in the patients with an APRI of <0.40 ($18.6 \pm 5.8 \times 10^4/\mu L$). In addition, platelet counts in many patients with an APRI of $\geq 0.40$ were $>10 \times 10^4/\mu L$, which indicated severely advanced hepatic fibrosis. Candidates for IFN treatment are recommended to have a platelet count of more than $10 \times 10^4/\mu L$ [39]. IFN treatment should be considered not only in patients with significant liver fibrosis, but also in patients with CH-C, mild liver fibrosis and undergoing HD. Furthermore, type IV collagen 7S of $\geq 5$ ng/mL and/or P-III-P of $\geq 5$ U/mL, which we herein propose, would be useful markers for distinguishing CH-C and for initiation of IFN treatment in relatively young patients with CH-C, undergoing HD, with a life expectancy of >5 years and without cardiovascular disease.

## ACKNOWLEDGEMENTS

Grants-in-Aid for Scientific Research (2011), Grant #23 590 979, Ministry of Education, Culture, Sports, Science and Technology, Japan.

## CONTRIBUTIONS

All listed authors contributed intellectually to the work presented here, through study concept and design, data acquisition, data analysis and interpretation, critical revision of the manuscript for important intellectual content, statistical analysis, funding or study supervision.

## CONFLICT OF INTERESTS

None.

## REFERENCES

1 Schiavon LL, Schiavon JL, Filho RJ *et al.* Simple blood tests as noninvasive markers of liver fibrosis in hemodialysis patients with chronic hepatitis C virus infection. *Hepatology* 2007; 46: 307–314.

2 Pereira BJ, Natov SN, Bouthot BA *et al.* Effects of hepatitis C infection and renal transplantation on survival in end-stage renal disease. The New England Organ Bank Hepatitis C Study Group. *Kidney Int* 1998; 53: 1374–1381.

3 Roth D, Hepatitis C. virus: the nephrologist's view. *Am J Kidney Dis* 1995; 25: 3–16.

4 Morales JM, Campistol JM. Transplantation in the patient with hepatitis C. *J Am Soc Nephrol* 2000; 11: 1343–1353.

5 Vosnides GG. Hepatitis C. in renal transplantation. *Kidney Int* 1997; 52: 843–861.
6 EBPG (European Expert Group on Renal Transplantation); European Renal Association (ERA-EDTA); European Society for Organ Transplantation (ESOT). European best practice guidelines for renal transplantation (part 1). *Nephrol Dial Transplant* 2000; 15(Suppl. 7): 1–85.
7 Covic A, Abramowicz D, Bruchfeld A *et al.* Endorsement of the Kidney Disease Improving Global Outcomes (KDIGO) hepatitis C guidelines: an European Renal Best Practice (ERBP) position statement. *Nephrol Dial Transplant* 2009; 24: 719–727.
8 Nakayama E, Akiba T, Marumo F, Sato C. Prognosis of anti-hepatitis C virus antibody-positive patients on regular hemodialysis therapy. *J Am Soc Nephrol* 2000; 11: 1896–1902.
9 Espinosa M, Martin-Malo A, Alvarez de Lara MA, Aljama P. Risk of death and liver cirrhosis in anti-HCV-positive long-term haemodialysis patients. *Nephrol Dial Transplant* 2001; 16: 1669–1674.
10 KDIGO. KDIGO clinical practice guidelines for the prevention diagnosis, evaluation, and treatment of hepatitis C in chronic kidney disease. *Kidney Int* 2008; 73(Suppl. 109): S1–S99.
11 The guideline for treatment of CH-C dialysis patients by Japanese Society for Dialysis Therapy. http://www.jsdt.or.jp/index_e.html
12 Murawaki Y, Ikuta Y, Okamoto K, Koda M, Kawasaki H. Diagnostic value of serum markers of connective tissue turnover for predicting histological staging and grading in patients with chronic hepatitis C. *J Gastroenterol* 2001; 36: 399–406.
13 Murawaki Y, Koda M, Okamoto K, Mimura K, Kawasaki H. Diagnostic value of serum type IV collagen test in comparison with platelet count for predicting the fibrotic stage in patients with chronic hepatitis C. *J Gastroenterol Hepatol* 2001; 16: 777–781.
14 Murawaki Y, Ikuta Y, Nishimura Y, Koda M, Kawasaki H. Serum markers for connective tissue turnover in patients with chronic hepatitis B and chronic hepatitis C. A comparative analysis. *J Hepatol* 1995; 23: 145–152.
15 Wai CT, Greenson JK, Fontana RJ *et al.* A simple noninvasive index can predict both significant fibrosis and cirrhosis in patients with chronic hepatitis C. *Hepatology* 2003; 38: 518–526.
16 Sterling RK, Lissen E, Clumeck N *et al.* Development of a simple noninvasive index to predict significant fibrosis in patients with HIV/HCV coinfection. *Hepatology* 2006; 43: 1317–1325.
17 Ono K, Ono T, Matsumata T. The pathogenesis of decreased aspartate aminotransferase and alanine aminotransferase activity in the plasma of hemodialysis patients: the role of vitamin B6 deficiency. *Clin Nephrol* 1995; 43: 405–408.
18 Barril G. Hepatitis C virus-induced liver disease in dialysis patients. *Nephrol Dial Transplant* 2000; 15 (Suppl. 8): 42–45.
19 Cotler SJ, Diaz G, Gundlapalli S *et al.* Characteristics of hepatitis C in renal transplant candidates. *J Clin Gastroenterol* 2002; 35: 191–195.
20 Luzar B, Ferlan-Marolt V, Brinovec V, Lesnicar G, Klopcic U, Poljak M. Does end-stage kidney failure influence hepatitis C progression in hemodialysis patients? *Hepatogastroenterology* 2003; 50: 157–160.
21 Sterling RK, Sanyal AJ, Luketic VA *et al.* Chronic hepatitis C infection in patients with end stage renal disease: characterization of liver histology and viral load in patients awaiting renal transplantation. *Am J Gastroenterol* 1999; 94: 3576–3582.
22 de Paula Farah K, Carmo RA, de Figueiredo Antunes CM *et al.* Hepatitis C, HCV genotypes and hepatic siderosis in patients with chronic renal failure on haemodialysis in Brazil. *Nephrol Dial Transplant* 2007; 22: 2027–2031.
23 Trevizoli JE, de Paula Menezes R, Ribeiro Velasco LF. Hepatitis C Is Less Aggressive in Hemodialysis Patients than in Nonuremic Patients. *Clin J Am Soc Nephrol* 2008; 3: 1385–1390.
24 Fabrizi F, Poordad FF, Martin P. Hepatitis C infection and the patient with end-stage renal disease. *Hepatology* 2002; 36: 3–10.
25 Meyers CM, Seeff LB, Stehman-Breen CO, Hoofnagle JH. Hepatitis C and renal disease: an update. *Am J Kidney Dis* 2003; 42: 631–657.
26 Yuki N, Ishida H, Inoue T *et al.* Reappraisal of biochemical hepatitis C activity in hemodialysis patients. *J Clin Gastroenterol* 2000; 30: 187–194.
27 Espinosa M, Martin-Malo A, Alvarez de Lara MA, Soriano S, Aljama P. High ALT levels predictviremia in anti-HCV-positive HD patients if a modified normal range of ALT is applied. *Clin Nephrol* 2000; 54: 151–156.
28 Fabrizi F, Lunghi G, Finazzi S *et al.* Decreased serum aminotransferase activity in patients with chronic renal failure: impact on the detection of viral hepatitis. *Am J Kidney Dis* 2001; 38: 1009–1015.
29 Manning DS, Afdhal NH. Diagnosis and quantitation of fibrosis. *Gastroenterology* 2008; 134: 1670–1681.
30 Murawaki Y, Ikuta Y, Koda M, Kawasaki H. Serum type III procollagen peptide, type IV collagen 7S domain, central triple-helix of type IV collagen and tissue inhibitor of metalloproteinases in patients with chronic viral liver disease: relationship to liver histology. *Hepatology* 1994; 20: 780–787.
31 Murawaki Y, Ikuta Y, Koda M, Nishimura Y, Kawasaki H. Clinical significance of serum hyaluronan in patients with chronic viral liver disease. *J Gastroenterol Hepatol* 1996; 11: 459–465.
32 Mahmoud IM, Sobh MA, El-Habashi AF *et al.* Interferon therapy in hemodialysis patients with chronic hepatitis C: study of tolerance, efficacy and posttransplantation course. *Nephron Clin Pract* 2005; 100: c133–c139.
33 Kamar N, Toupance O, Buchler M *et al.* Evidence that clearance of hepatitis C virus RNA after alpha-interferon therapy in dialysis patients is sustained after renal transplantation. *J Am Soc Nephrol* 2003; 14: 2092–2098.
34 Cruzado JM, Casanovas-Taltavull T, Torras J, Baliellas C, Gil-Vernet S, Grinyó JM. Pretransplant interferon

prevents hepatitis C virus-associated glomerulonephritis in renal allografts by HCV-RNA clearance. *Am J Transplant* 2003; 3: 357–360.

35 Glicklich D, Thung SN, Kapoian T, Tellis V, Reinus JF. Comparison of clinical features and liver histology in hepatitis C-positive dialysis patients and renal transplant recipients. *Am J Gastroenterol* 1999; 94: 159–163.

36 Hu KQ, Lee SM, Hu SX, Xia VW, Hillebrand DJ, Kyulo NL. Clinical presentation of chronic hepatitis C in patients with end-stage renal disease and on hemodialysis versus those with normal renal function. *Am J Gastroenterol* 2005; 100: 2010–2018.

37 Martin P, Carter D, Fabrizi F *et al.* Histopathological features of hepatitis C in renal transplant candidates. *Transplantation* 2000; 69: 1479–1484.

38 Sezer S, Ozdemir BH, Arat Z, Turan M, Ozdemir NF, Haberal M. Spectrum of liver damage and correlation with clinical and laboratory parameters in HCV infected hemodialysis patients. *Ren Fail* 2001; 23: 807–818.

39 Bruno S, Stroffolini T, Colombo M *et al.* Italian Association of the Study of the Liver Disease (AISF). Sustained virological response to interferon-alpha is associated with improved outcome in HCV-related cirrhosis: A retrospective study. *Hepatology* 2007; 45: 579–587.

PLOS | ONE

# Tumor Necrosis Factor-α Promotes Cholestasis-Induced Liver Fibrosis in the Mouse through Tissue Inhibitor of Metalloproteinase-1 Production in Hepatic Stellate Cells

**Yosuke Osawa[1,2]*, Masato Hoshi[3], Ichiro Yasuda[2], Toshiji Saibara[4], Hisataka Moriwaki[2], Osamu Kozawa[1]**

1 Department of Pharmacology, Gifu University Graduate School of Medicine, Gifu, Gifu, Japan, 2 Department of Gastroenterology, Gifu University Graduate School of Medicine, Gifu, Gifu, Japan, 3 Faculty of Health Science, Suzuka University of Medical Science, Suzuka, Mie, Japan, 4 Department of Gastroenterology and Hepatology, Kochi University School of Medicine, Nankoku, Kochi, Japan

## Abstract

Tumor necrosis factor (TNF)-α, which is a mediator of hepatotoxicity, has been implicated in liver fibrosis. However, the roles of TNF-α on hepatic stellate cell (HSC) activation and liver fibrosis are complicated and remain controversial. To explore this issue, the role of TNF-α in cholestasis-induced liver fibrosis was examined by comparing between TNF-$\alpha^{-/-}$ mice and TNF-$\alpha^{+/+}$ mice after bile duct ligation (BDL). Serum TNF-α levels in mice were increased by common BDL combined with cystic duct ligation (CBDL+CDL). TNF-α deficiency reduced liver fibrosis without affecting liver injury, inflammatory cell infiltration, and liver regeneration after CBDL+CDL. Increased expression levels of collagen α1(I) mRNA, transforming growth factor (TGF)-β mRNA, and α-smooth muscle actin (αSMA) protein by CBDL+CDL in the livers of TNF-$\alpha^{-/-}$ mice were comparable to those in TNF-$\alpha^{+/+}$ mice. Exogenous administration of TNF-α decreased collagen α1(I) mRNA expression in isolated rat HSCs. These results suggest that the reduced fibrosis in TNF-$\alpha^{-/-}$ mice is regulated in post-transcriptional level. Tissue inhibitor of metalloproteinase (TIMP)-1 plays a crucial role in the pathogenesis of liver fibrosis. TIMP-1 expression in HSCs in the liver was increased by CBDL+CDL, and the induction was lower in TNF-$\alpha^{-/-}$ mice than in TNF-$\alpha^{+/+}$ mice. Fibrosis in the lobe of TIMP-$1^{-/-}$ mice with partial BDL was also reduced. These findings indicate that TNF-α produced by cholestasis can promote liver fibrosis via TIMP-1 production from HSCs. Thus, targeting TNF-α and TIMP-1 may become a new therapeutic strategy for treating liver fibrosis in cholestatic liver injury.

**Citation:** Osawa Y, Hoshi M, Yasuda I, Saibara T, Moriwaki H, et al. (2013) Tumor Necrosis Factor-α Promotes Cholestasis-Induced Liver Fibrosis in the Mouse through Tissue Inhibitor of Metalloproteinase-1 Production in Hepatic Stellate Cells. PLoS ONE 8(6): e65251. doi:10.1371/journal.pone.0065251

**Editor:** Simon Afford, University of Birmingham, United Kingdom

**Received** January 14, 2013; **Accepted** April 23, 2013; **Published** June 3, 2013



**Funding:** This work was supported by grants from the Takeda Science Foundation, the Kondou Kinen Medical Foundation, the Kurozumi Medical Foundation, the Yasuda Medical Foundation, the Senshin Medical Research Foundation, and by a Grant-in-Aid for Scientific Research from the Ministry of Education, Science, Sports, and Culture of Japan (23790787). The funders had no role in study design, data collection and analysis, decision to publish, or preparation of the manuscript.

**Competing Interests:** The authors have declared that no competing interests exist.

* E-mail: osawa-gif@umin.ac.jp

## Introduction

Chronic liver injury is characterized by hepatocyte cell death, hepatic inflammation, and activation of hepatic stellate cell (HSC), a major fibrogenic cell type in the liver [1]. Advanced liver fibrosis disrupts the normal architecture of the liver, causing hepatocellular dysfunction and portal hypertension. Cholestasis is associated with many liver diseases, and bile duct ligation (BDL) has been used in an animal model of chronic liver injury because it duplicates the hepatocyte damage, HSC activation, and liver fibrosis observed in human liver diseases. In the BDL model, accumulation of bile acids by biliary obstruction is thought to contribute to the liver damage [2,3]. Bile acids are amphipathic molecules synthesized by hepatocytes and have detergent action required for lipid absorption. Exposure of hepatocytes to elevated concentrations of bile acid results in cell death [3,4], and bile acid-associated death receptor-mediated cell death is one of the common mechanism for cholestatic hepatocyte injury [5]. Tumor necrosis factor (TNF)-α, which is the mediator of hepatotoxicity in many liver diseases [6], is elevated by common BDL (CBDL) [7], and the liver injury and fibrosis induced by CBDL are reduced in TNF-$\alpha^{-/-}$ mice [8] and TNF receptor (TNFR)$1^{-/-}$ mice [9]. In addition, liver fibrosis induced by carbon tetrachloride ($CCl_4$) is also reduced in TNFR$1^{-/-}$ mice [10]. Thus, TNF-α has been thought to be crucial for liver injury and subsequent liver fibrosis. However, TNF-α alone does not induce hepatocyte cell death, and the sensitization of hepatocytes by D-galactosamine (GalN) is required for TNF-α-induced liver injury in mice [11,12]. In contrast to its negative regulatory effects, TNF-α has a protective role in liver injury [13] and is required for liver regeneration [14]. Furthermore, TNF-α inhibits collagen α1(I) mRNA expression in HSCs [15,16,17]. Thus, the roles of TNF-α on HSCs activation and liver fibrosis are complicated and remain controversial.

Progression of liver fibrosis is associated with the inhibition of matrix degradation [18]. Matrix degradation is induced by the matrix metalloproteinase (MMP) family of enzymes; MMP-2, -3, and -9 are associated with the liver. Tissue inhibitor of metalloproteinase (TIMP)-1, the most important endogenous inhibitor of most MMPs, plays a crucial role in the pathogenesis of liver fibrosis, and its expression in HSCs is enhanced by TNF-α [9,19,20]. In human liver fibrosis, TIMP-1 expression is increased compared to that in the normal liver [18]. Overexpression of

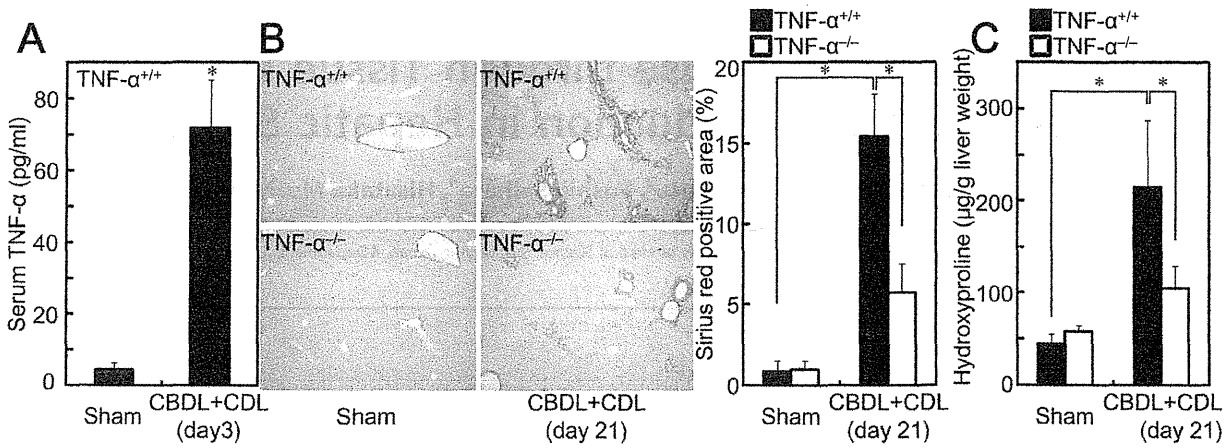


**Figure 1. TNF-α deficiency reduced liver fibrosis after CBDL+CDL.** TNF-$\alpha^{+/+}$ and TNF-$\alpha^{-/-}$ mice received CBDL+CDL. The animals were sacrificed on 3 (A) or 21 (B, C) days after the surgery. (A) Serum TNF-α levels were measured by ELISA. (B, C) Collagen deposition was assessed by Sirius red staining (B, original magnification: 40×, graph in right panel) and measurement of hydroxyproline content (C). Data are mean ± SD from at least 5 independent experiments. *, $P<0.05$ using a 2-tailed Student's t-test.
doi:10.1371/journal.pone.0065251.g001

MMP-9 in the mouse liver, using an adenovirus vector, reduces liver fibrosis after $CCl_4$ treatment [21]. Moreover, antagonization of TIMP-1 by a catalytically inactive mutant MMP-9 [21] or by TIMP-1 neutralizing antibody [22] decreases liver fibrosis. Inversely, transgenic mice overexpressing TIMP-1 in the liver show increased liver fibrosis after $CCl_4$ treatment, whereas TIMP-1 overexpression alone does not result in liver fibrosis [23]. In addition to its role in inhibiting matrix degradation, TIMP-1 promotes survival and proliferation of liver cells. TIMP-$1^{-/-}$ mice demonstrate impaired liver injury and hepatocyte proliferation after hepatic ischemia and reperfusion [24] and demonstrate exacerbated liver injury and fibrosis induced by $CCl_4$ [25]. Thus, the effects of TIMP-1 on liver injury and fibrosis depend on pathophysiological condition, and its role on fibrosis after cholestatic liver injury remains unclear. To attempt to clarify the precise roles, this study investigated the involvement of TNF-α and TIMP-1 in the progression of fibrosis after cholestatic liver injury.

## Materials and Methods

### Ethics Statement

The experiments were conducted in accordance with the institutional guidelines and the protocol was approved by the Animal Research Committee of Gifu University (Permit Numbers: 23-3 and 23-38). All surgery was performed under anesthesia, and all efforts were made to minimize suffering.

### Animals

Wister male rats and male wild-type mice (C57Bl/6J), TNF-α-deficient mice (TNF-$\alpha^{-/-}$), and TIMP-1-deficient mice (TIMP-$1^{-/-}$) were used for this study. TNF-$\alpha^{-/-}$ mice (#5540, C57Bl/6 background) and TIMP-$1^{-/-}$ mice (#6243, C57Bl/6 background) were obtained from Jackson Laboratory (Bar Harbor, ME, USA), and wild-type C57Bl/6J mice and Wister male rats were from Japan SLC (Shizuoka, Japan).

### Bile Duct Ligation (BDL)

Eight-10 week-old male mice were used for studies. To perform common BDL and cystic duct ligation (CBDL+CDL), the peritoneal cavity was opened under anesthesia and the common bile duct was double ligated below the bifurcation, single ligated above the pancreas, and cut between the ligatures. In addition, the cystic duct was single ligated. The left hepatic duct was single ligated for partial BDL (PBDL) as previously reported [26,27]. As necessary, GalN (Nacalai Tesque, Kyoto, Japan) (20 mg/mouse) was intraperitoneally administrated at 30 min before the surgery. On days 1, 3, 7, 21 after the surgery, mice were humanely killed.

### Measurement of Serum TNF-α

Mouse serum TNF-α level was measured by ELISA (Thermo Scientific, Rockford, IL, USA).

### Histological Analysis

The liver was fixed with 10% formalin, sectioned, and stained with H&E. Collagen deposition was stained with Sirius red (saturated picric acid containing 0.1% DirectRed 80 and 0.1% FastGreen FCF). The Sirius red positive area was quantitated using the ImageJ software (U.S. National Institutes of Health; http://rsb.info.nih.gov/ij/) and shown as a percentage of the total section area. Apoptosis was assessed by the terminal deoxynucleotidyl transferase-dUTP nick end labeling (TUNEL) assay (Promega, Madison, WI, USA, #G7132). The number of TUNEL positive nuclei was determined in 10 randomly selected fields. F4/80, CD3, Ki67, TIMP-1, and desmin were stained with anti-F4/80 (Santa Cruz Biotechnology, Santa Cruz, CA, USA, sc-52664), CD3 (Abcam, Cambridge, MA, USA, ab16669), Ki67 (Thermo scientific, RM-9106), TIMP-1 (R&D Systems, Minneapolis, MN, USA), desmin (Lab Vision, Fremont, CA, USA) antibodies using the Vectastain Elite ABC Kit (Vector Laboratories, Burlingame, CA, USA). Diaminobenzidine tetrahydrochloride was used as peroxidase substrate and sections were counterstained with hematoxylin. The immunostained-positive area of F4/80 was determined using ImageJ software and shown as a percentage of the total section area. The number of CD3 or Ki67-expressing cells was determined in 10 randomly selected fields. In some experiments, fluorescent-dye labeled secondary antibodies (Alexa Fluor 488 anti-rabbit for desmin and Alexa Fluor 594 anti-goat for TIMP-1) (Invitrogen, Carlsbad, CA, USA) were used for detection of primary antibodies as previously reported [28].